HELSINKI UNIVERSITY OF TECHNOLOGY
Department of Electrical and Communications Engineering
Radio Laboratory

MIKKO KYRÖ

MULTI – ELEMENT ANTENNA FOR DVB – H TERMINAL

Thesis submitted in partial fulfilment for the degree of Master of Science in Espoo . .2007

Supervisor

Prof. Pertti Vainikainen

Instructor

M.Sc. (Tech.) Maria Mustonen

HELSINKI UNIVERSITY OF TECHNOLOGY **ABSTRACT OF THE MASTER'S THESIS**

Author:	Mikko Kyrö
Name of the thesis:	Multi-element Antenna for DVB-H Terminal
Date:	22.10.2007 **Number of pages**: 80
Department:	Department of Electrical and Communications Engineering
Professorship:	S-26 Radio Engineering
Supervisor:	Professor Pertti Vainikainen
Instructor:	M.Sc. (Tech.) Maria Mustonen

In this thesis feasibility to implement multi-element antenna configurations in handheld digital television receivers (Digital Video Broadcasting – Handheld (DVB-H)) has been studied. A two-element antenna for a DVB-H terminal was designed, manufactured and the performance of the antenna was evaluated with simulations and measurements.

The use of multi-element antenna systems such as multiple-input multiple-output (MIMO) can enhance the mutual information or reliability of the wireless communications link compared to a single-element antenna system. The drawback of using the MIMO system is the increased complexity of the transceiver. The DVB-H system works at about 470 – 800 MHz frequency range and the relative bandwidth is very broad. This makes antenna designing challenging because an internal antenna in a handheld terminal is inevitably electrically small and broad bandwidth is difficult to achieve. In addition, in a handheld terminal there are very few places where DVB-H antennas can be located. Due to low frequency and small size of the terminal it is difficult to implement uncorrelated antenna elements.

In this work antenna elements were realized with a coupling element based antenna structure. These antennas are tuned to resonance with a matching circuit. At first achievable bandwidths and envelope correlation coefficients of different antenna element structures and their locations were investigated with simulations. Finally, the multi-element antenna was implemented with two antenna elements which were located in the corners of the ground plane at the same short side. The ground plane represents the circuit board of the terminal. In this thesis a narrow-band single-resonant matching circuit was designed to evaluate the performance of the antenna with measurements and a broad-band dual-resonant matching circuit to cover the whole DVB-H band. Because the size of the antenna structure was desired to be small, the DVB-H band was divided into two parts and separate matching circuits were designed for both sub-bands. In the final antenna the desired matching circuit would be selected with RF switches. With this procedure, the realized gain specification of the DVB-H antennas was fulfilled with a 2.5 dB margin in simulations and measurements.

The MIMO performance of the dual-element antenna structure was evaluated in realistic propagation environments with an antenna analysis tool called measurement based antenna testbed (MEBAT). A single-element reference antenna was designed for the MEBAT simulations in order to gain knowledge whether it is useful to have several antenna elements in a DVB-H receiver. According to simulation results, the greatest benefit from the use of the dual-element antenna is attained at high reliability levels. In that case the mutual information of a 2 x 2 MIMO system can be two to four times higher than with a single-input single-output (SISO) configuration. At lower reliability level the difference is smaller. The performance of the MIMO system does not depend only on the signal environment but also on the orientation of the receiving antenna and on the polarizations of the transmitting antennas. These matters were also investigated with MEBAT simulations.

Keywords: DVB-H, electrically small antenna, matching circuit, coupling element based antenna structure, multi-element antenna, realized gain, mutual information

TEKNILLINEN KORKEAKOULU **DIPLOMITYÖN TIIVISTELMÄ**

Tekijä:	Mikko Kyrö
Työn nimi:	Monielementtiantenni DVB-H-vastaanottimeen
Päivämäärä:	22.10.2007 **Sivumäärä**: 80
Osasto:	Sähkö- ja tietoliikennetekniikan osasto
Professuuri:	S-26 Radiotekniikka
Valvoja:	Professori Pertti Vainikainen
Ohjaaja:	DI Maria Mustonen

Tässä diplomityössä tutkittiin monielementtiantennien käyttökelpoisuutta kannettavissa Digital Video Broadcasting – Handheld (DVB-H)-digitaalitelevisiovastaanottimissa. Työssä suunniteltiin ja valmistettiin kaksielementtiantenni DVB-H-käyttöön. Antennin toimintaa arvioitiin simuloinneilla ja mittauksilla.

Monielementtiantennijärjestelmien, kuten multiple-input multiple-output (MIMO), käyttö mahdollistaa radiotietoliikenneyhteyden kapasiteetin kasvun tai niillä voidaan lisätä yhteyden luotettavuutta verrattuna perinteiseen yhden vastaanotin- ja lähetysantennin järjestemään. MIMO-järjestelmän haittapuolena voidaan pitää lähettimen ja vastaanottimen rakenteen monimutkaistumista. DVB-H-signaalin vastaanotto tapahtuu matalalla taajuudella ja leveällä taajuuskaistalla (noin. 470 – 800 MHz), mikä tekee pienen laitteen antennisuunnittelusta haastavaa. Kannettavan TV-vastaanottimen sisäisistä antenneista tulee väistämättä sähköisesti pieniä ja laajakaistaista toimintaa on vaikea saavuttaa. Lisäksi nykyaikaisessa kannettavassa päätelaitteessa on hyvin rajallinen määrä paikkoja, joihin DVB-H-antennit voidaan sijoittaa. Matalasta taajuudesta ja laitteen pienestä koosta johtuen korreloimattomia antennielementtejä on vaikea toteuttaa.

Tässä työssä antennit toteutettiin kytkentäelementteihin perustuvalla antennirakenteella, jossa antenni viritetään resonanssiin sovituspiirin avulla. Eri antennirakenteilla ja elementtien sijoittelulla saavutettavia kaistanleveyksiä sekä verhokäyrä-korrelaatioita tutkittiin aluksi simuloinneilla. Lopulta päädyttiin käyttämään kahta antennielementtiä, jotka asetettiin päätelaitteen piirilevyä kuvaavan maatason nurkkiin samalle lyhyelle sivulle. Työssä suunniteltiin kapeakaistainen yksiresonanssisovituspiiri mittauksia varten, sekä leveäkaistainen kaksoisresonanssisovituspiiri kattamaan koko DVB-H-taajuuskaista. Koska antennirakenteesta haluttiin pieni, jouduttiin DVB-H-kaista jakamaan kahteen osaan ja suunnittelemaan sovituspiirit erikseen molemmille osakaistoille. Lopullisessa antennissa haluttu sovituspiiri valittaisiin RF-kytkimillä. Tällä menettelyllä DVB-H-antenneille asetettu toteutuneen vahvistuksen spesifikaatio ylitettiin 2.5 dB:n marginaalilla sekä simuloinneissa että mittauksissa.

Antennirakenteen MIMO-toimintaa tutkittiin measurement based antenna testbed (MEBAT) -nimisellä antennievaluaatiotyökalulla. MEBAT:in avulla kaksielementtiantennin toimintaa voitiin simuloida realistisessa etenemisympäristöissä. Simulointeja varten suunniteltiin yksielementtinen referenssiantenni, jotta voitiin selvittää, onko useamman elementin käytöstä hyötyä. Simulointituloksista ilmenee, että suurin hyöty kaksielementtiantennin käytöstä saavutetaan suurilla luotettavuustasoilla. Tällöin käyttämällä 2 x 2 MIMO-järjestelmää keskinäisinformaatio voi olla noin kaksin-nelinkertainen verrattuna single-input single-output (SISO)-konfiguraatioon. Matalammilla luotettavuustasoilla ero on pienempi. MIMO-järjestelmän suorituskykyyn vaikuttavat käyttöympäristön lisäksi myös vastaanottoantennin asento sekä lähetysantennissa käytettävät polarisaatiot. Myös näitä asioita tutkittiin MEBAT-simuloinneilla.

Avainsanat: DVB-H, sähköisesti pieni antenni, sovituspiiri, kytkentäelementtiin perustuva antennirakenne, monielementtiantenni, toteutunut vahvistus, keskinäisinformaatio

PREFACE

Work for this Master's thesis was carried out in the Radio Laboratory of Helsinki University of Technology (TKK).

At first, I would like to express my gratitude to my supervisor, professor Pertti Vainikainen, for his invaluable comments and guidance during the work. I would also like to thank him for giving me an opportunity to work with this interesting topic.

My special thanks belong to my instructor, Maria Mustonen, for her comments and suggestions related to the thesis. She had always time for my questions that most often concerned Matlab, MEBAT or matters related to MIMO.

I would like to thank Jari Holopainen and Clemens Icheln for constructive comments concerning the work. I am also grateful to Pekka Talmola from Nokia for sharing his expertise in the DVB-H system. In addition, I would like to thank my colleagues in the Radio Laboratory for a friendly working atmosphere.

My parents, Maarit and Pentti deserve warm thanks for supporting and encouraging my throughout my studies.

Finally, I would like to thank my girlfriend Nina for her love and support.

Espoo, October 19, 2007

Mikko Kyrö

TABLE OF CONTENTS

LIST OF ABBREVIATIONS

AUT	antenna under test
CENELEC	European Committee for Electrotechnical Standardization
DVB	Digital Video Broadcasting
DVB-C	Digital Video Broadcasting -Cable
DVB-H	Digital Video Broadcasting – Handheld
DVB-S	Digital Video Broadcasting -Satellite
DVB-T	Digital Video Broadcasting –Terrestrial
EPWBM	experimental plane wave based method
ETSI	European Telecommunications Standards Institute
FEC	forward error correction
GSM	Global System for Mobile Communications
IE3D	electromagnetic simulator based on the method of moments by Zeland Software, Inc.
MEBAT	measurement based antenna testbed
MPE	multiprotocol encapsulation
MIMO	multiple-input multiple-output
MISO	multiple-input single-output
PCB	printed circuit board
PIFA	planar inverted – F antenna
Rx	receiver
SAR	specific absorption rate
SIMO	single-input multiple-output
SISO	single-input single-output
SNR	signal-to-noise ratio
SPDT	single pole, double throw

TKK	Helsinki University of Technology
Tx	transmitter
UMTS	Universal Mobile Telecommunications System
VNA	vector network analyser
WLAN	Wireless Local Area Network

LIST OF SYMBOLS

B	susceptance
B_{hp}	half power bandwidth
B_r	relative bandwidth
$B_{r,crit}$	relative bandwidth achieved by critical coupling
$B_{r,max}$	maximum relative bandwidth
C	capacitance
D	directivity
d	distance between the load and the tuning stub
f	frequency
f_c	centre frequency
f_r	resonant frequency
G	conductance or gain
G_{AUT}	realized gain of the antenna under test
G_r	realized gain
G_{ref}	realized gain of the reference antenna
k	wave number
L	inductance
L_{refl}	reflection loss
l	length of a tuning stub
n_r	number of receiving antennas
n_t	number of transmitting antennas
P_{AUT}	power received by the antenna under test
P_{in}	power accepted by the antenna
P_l	power loss in the resonator structure
P_{rad}	radiated power

P_{refl}	reflected power
P_{ref}	power received by the reference antenna
P_t	total incident power
Q	quality factor
Q_0	unloaded quality factor
Q_d	quality factor for dielectric losses
Q_l	loaded quality factor
Q_m	quality factor for conductivity losses
Q_{rad}	radiation quality factor
R_L	real part of the load impedance
r	radius of the smallest sphere enclosing an antenna
S	voltage standing wave criterion or power density
T	coupling coefficient
t	time
$VSWR$	voltage standing wave ratio
W	energy stored in a resonator
X	reactance
X_L	reactance of a load
Y_L	admittance of a load
Y_0	admittance of a transmission line
y	normalized admittance
Z_A	impedance of a antenna structure
Z_0	impedance of a transmission line
Z_L	impedance of a load
$\tan \delta$	loss tangent
ε	permittivity
ε_r	relative permittivity

η_{rad}	radiation efficiency
η_{tot}	total efficiency
η_m	matching efficiency
λ	wavelength
λ_0	wavelength in vacuum
μ	permeability
ρ	reflection coefficient
ρ_m	matching criterion defined by reflection coefficient
ω	angular frequency
σ	conductivity

1 INTRODUCTION

Mobile digital television (DTV) represents one of the latest major additions to the features of mobile terminals. Digital Video Broadcasting – Handheld (DVB-H) is one of the technologies bringing mobile television to a handheld terminal. DVB-H is a relatively new technology and quite a few antenna solutions have been developed for it. Internal DVB-H antennas are electrically small and this leads to low total antenna efficiency and moderate performance of the receiver. Because the handheld DVB-H device operates only as a receiver, this can be tolerated as long as the signal-to-noise ratio (SNR) is sufficient. SNR depends on the signal environment and it can be improved by adding signal power or using a better antenna. Electromagnetic interference caused by computers and other electronic devices degreases SNR especially in urban environment.

The goal of this thesis is to gain knowledge on the feasibility of multi-element antenna solutions for a DVB-H terminal. The reason for the use of multi-element antenna systems e.g. multiple-input multiple-output (MIMO) is that they can enhance the mutual information and reliability of wireless communications. However, it is challenging to implement multiple electrically small antennas with low correlation in a handheld device. The most promising technique to realize this is polarization diversity. Commercial multi-element antennas have been developed e.g. for Wireless Local Area Network (WLAN) but not for systems operating below 1 GHz. Advanced solutions have also been developed for Universal Mobile Telecommunications System (UMTS) but they are not yet used in commercial products. Before DVB-H there has not been any need to implement multi-element antenna systems at low frequencies because older systems like Global System for Mobile Communications (GSM) 900 do not need the increase of the mutual information that can be attained with multi-element antennas.

In the Chapter 2 basic parameters of the small antennas and their limitation on size reduction are presented. Design principles of the matching circuits and bandwidth enhancement methods are also described in Chapter 2. Multi-element antenna solutions are investigated in Chapter 3. DVB-H system and current antenna solutions for DVB-H terminals are introduced in Chapter 4. The design process of a multi-element antenna prototype is presented in Chapter 5. This includes optimization of the antenna structure and the different matching circuits. Chapter 6 introduces the simulation and the measurement results of the prototype antenna. In Chapter 7 the MIMO performance of the prototype antenna is evaluated with an antenna evaluation tool called the measurement-based antenna test bed (MEBAT). Chapter 8 presents the final conclusions of the thesis.

2 BASICS OF SMALL ANTENNAS

An antenna is a device that can transmit and receive electromagnetic waves. Modern mobile communications systems set many demands especially for antennas in the terminals. Antennas are required to be small, low-cost, but yet achieve high performance and have characteristics like operation in several frequency bands and wide bandwidth. In this chapter the basics of small antennas are presented.

An electrically small antenna is small compared to the wavelength at the operating frequency. Therefore, a physically large antenna can be electrically small if it is operating at low frequency. Usually the dimensions of the electrically small antenna are below $\lambda_0/4$, where λ_0 is the wavelength in free space [1]. Another definition is that the size of the electrically small antenna is relative to radianlength ($\lambda/2\pi$) so that it fits inside a sphere with radius equal to radianlength [2]. The free space wavelength at DVB-H band is about 0.64 – 0.37 m and an internal antenna for a handheld mobile terminal is inevitably electrically small.

2.1 Antenna impedance and reflection from a mismatched load

The impedance of the antenna is the impedance presented by the antenna from its input terminal. The impedance consists of real and imaginary parts and it can be measured using e.g. a vector network analyser (VNA). If the antenna impedance Z_A differs from the transmission line impedance Z_0, a reflection occurs (see Figure 2.1). A part of the power that is fed to the antenna reflects from a discontinuation of impedances and the rest of the power is absorbed by the antenna. The voltage reflection coefficient is defined as [3]

$$\rho = \frac{Z_A - Z_0}{Z_A + Z_0}. \tag{2.1}$$

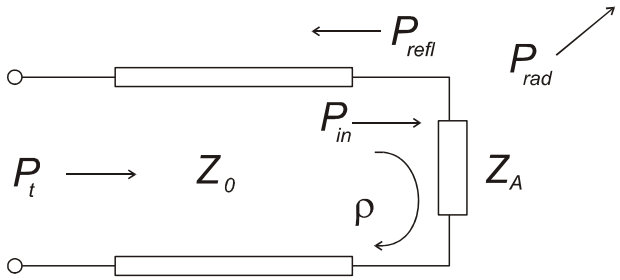

Figure 2.1: *Reflection from a mismatched load. P_t is the total incident power, P_{in} is the power accepted by the antenna, P_{refl} is the power reflected from load and P_{rad} is the power radiated.*

For a single-port device like antenna the reflection coefficient ρ corresponds to the scattering parameter S_{11}. Reflections are not desired because then a part of the power is not absorbed into the antenna. Power is proportional to the square of the voltage and therefore the power reflection coefficient is $|\rho|^2 = P_{refl} / P_t$. The power loss due to reflections in decibels, called the reflection loss L_{refl} is [3]

$$L_{refl} = 10\log\frac{1}{1-|\rho|^2}. \tag{2.2}$$

The return loss describes how much smaller the reflected power P_{refl} is compared to the power accepted by the antenna P_{in} in decibels [3]

$$L_{retn} = 10\log\frac{1}{|\rho|^2}. \tag{2.3}$$

Reflections from the antenna form a standing wave in the feed line. The ratio of the maximum voltage and minimum voltage is called the voltage standing wave ratio (VSWR). If the reflection coefficient is known, the *VSWR* can be calculated from [3]

$$\mathrm{VSWR} = \frac{1+|\rho|}{1-|\rho|}. \tag{2.4}$$

The antenna impedance can be matched to the transmission line impedance. However, this can be done only in a narrow frequency range. Impedance matching techniques are described in Section 2.4.

2.2 Quality factors and achievable impedance bandwidth

The impedance of the small antennas has a large reactive component, because a small antenna stores relatively large amount of energy but does not radiate very well. In order to deliver power with the antenna it has to be tuned to resonance which means that the reactive component of the antenna impedance has to be cancelled out and the resonance resistance must be transformed to match the transmission line impedance Z_0. Tuning can be done with a matching circuit or by designing the antenna structure so that the antenna is self-resonant. However, sufficient reactance cancellation can only occur inside a narrow bandwidth.

The small antennas can be modeled as resonators and the quality factors can be used to examine the impedance bandwidth and different loss mechanisms of the small antennas. Before defining quality factors a brief review of the resonators is needed. A resonator is a device that has a

natural oscillating frequency. A resonator can be modeled as a parallel (see Figure 2.2) or a series resonance circuit. The natural resonant frequency of the resonator is [3]

$$f_r = \frac{1}{2\pi\sqrt{LC}}, \tag{2.5}$$

where L stands for the inductance and C for the capacitance of the resonance circuit.

If energy is fed to the circuit at the resonance frequency f_r, the energy stored in the circuit grows. However, due to losses in the circuit, the energy does not increase indefinitely. The resonator theory can be used to evaluate the ratio between energy radiated by an antenna and energy stored in the antenna structure. The antenna can be modeled by a resonant equivalent circuit (see Figure 2.2).

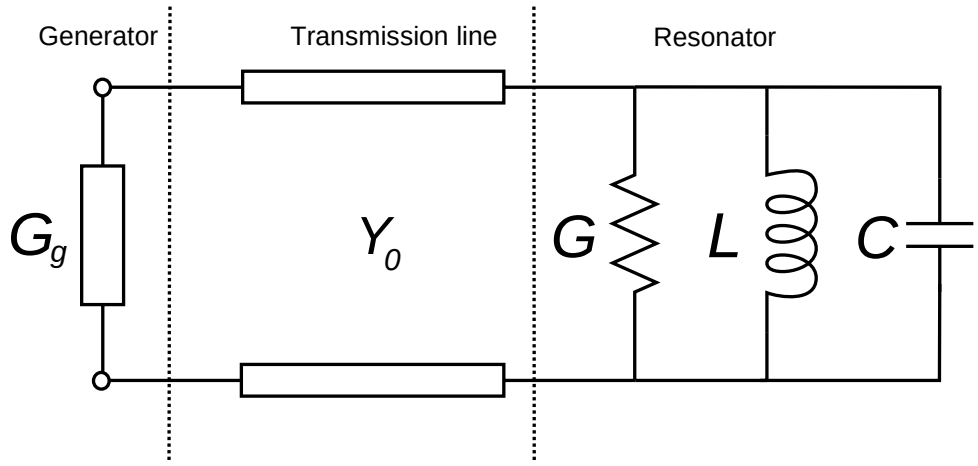

Figure 2.2: *A parallel resonance circuit with the generator admittance G_g and the transmission line admittance Y_0. The admittance of the resonator consists of the conductance G, the inductance L and the capacitance C.*

The quality factor Q describes the ratio between the energy stored and the power losses of the resonator and it is generally defined as [3]

$$Q = \frac{2\pi \cdot fW}{P_l}, \tag{2.6}$$

where f is the frequency, W is the energy stored in the resonator and P_l is the power loss in the resonator. A high quality factor means that the resonance is sharp and the bandwidth is narrow. The purpose of the antenna is to couple to free space wave. This means that the power stored in the antenna should be minimized and the radiating losses maximized.

The loss power in the resonator can be separated into different parts and corresponding quality factors can be defined. Unloaded quality factor represents losses of the resonator and it can be written as a sum [4]:

$$\frac{1}{Q_0} = \frac{1}{Q_d} + \frac{1}{Q_m} + \frac{1}{Q_{rad}}, \tag{2.7}$$

where Q_d represents dielectric losses, Q_m conductivity losses and Q_{rad} radiating losses. Unloaded quality factor can not be measured directly because the resonator must be connected to the measurement circuit. The measured quality factor includes external losses and is called the loaded quality factor Q_l. It can be calculated from [4]

$$\frac{1}{Q_l} = \frac{1}{Q_0} + \frac{1}{Q_{ext}}, \tag{2.8}$$

where Q_{ext} represent losses that are produced in the circuit outside of the resonator.

Loaded quality factor can be calculated from the resonant frequency f_r and half-power bandwidth B_{hp} as [4]

$$Q_l = \frac{f_r}{B_{hp}}. \tag{2.9}$$

As shown in Figure 2.3 the half-power bandwidth is defined as the frequency range with the reflection coefficient (see Equation (2.1)) $|\rho|^2 \leq \frac{1+|\rho_r|^2}{2}$.

We can now evaluate the unloaded quality factor Q_0 from [4]

$$Q_0 = \frac{2Q_l}{1 \pm |\rho_r|}. \tag{2.10}$$

In the denominator the plus sign is used when the resonator is undercoupled and the minus when it is overcoupled. When the losses of the resonator are greater than the losses of the external circuit $Q_e > Q_0$ ($G_g < G$), the resonator is undercoupled. If the losses of the external circuit are greater than the losses of the resonator $Q_e < Q_0$ ($G_g > G$), the resonator is overcoupled.

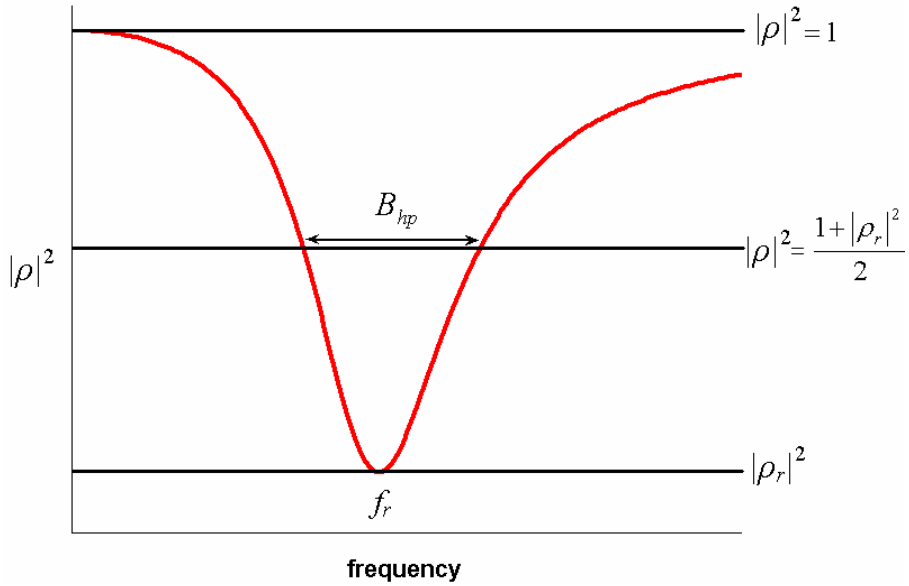

Figure 2.3: *The relation between the half power bandwidth B_{hp} and the reflection coefficient ρ.*

For the small antennas, the bandwidth is limited only by the resonance behavior of the input impedance [5]. If the matching criterion is chosen to be $VSWR \leq S$ and f_1 and f_2 are the lower and the upper limit of the frequency band, respectively, so that $VSWR\ (f_1) = VSWR\ (f_2) = S$ and f_c is the arithmetic center frequency of the frequency band the relative impedance bandwidth is defined as

$$B_r = \frac{f_2 - f_1}{f_c}. \tag{2.11}$$

The theoretical maximum achievable relative impedance bandwidth with a certain matching criterion is defined by the Bode-Fano criterion [6]

$$B_{r,\max} = \frac{\pi}{Q_0 \ln\left(1/|\rho_m|\right)}, \tag{2.12}$$

where ρ_m is the maximum value of the reflection coefficient that is acceptable over the passband. An antenna that fulfils the Bode-Fano criterion can not be implemented with real antennas and it requires infinite number of reactive matching components.

In [7] the theoretical maximum relative impedance bandwidth of a resonant antenna having a certain Q_0 and a matching circuit comprising a different number of additional lossless resonators has been investigated (see Figure 2.4). Small antennas are not usually in resonance and they have to be tuned to resonance with single-resonant matching circuit. In Figure 2.4 this corresponds to the $n = 1$ curve. If the second resonator is added, about 100 % improvement of

relative bandwidth can be attained in ideal case [7]. After this the improvement in bandwidth saturates rapidly towards the Bode-Fano criterion $n = \infty$ (2.12) with increasing number of resonators.

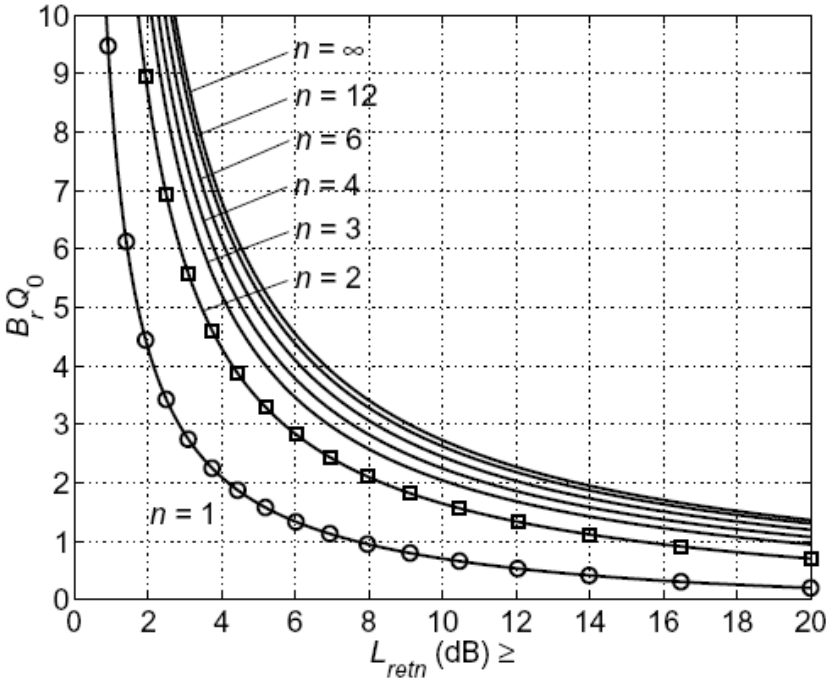

Figure 2.4: *The theoretical maximum achievable bandwidth $B_{r,max}$ of a resonant antenna with a certain Q_0 and a matching circuit comprising of n-1 additional resonators as a function of the minimum required return loss L_{retn}. [7]*

For the single-resonant matching (see Section 2.4.1) the connection between the unloaded quality factor and the achievable bandwidth is given as [5]

$$B_r = \frac{1}{Q_0}\sqrt{\frac{(TS-1)(S-T)}{S}}, \tag{2.13}$$

where the VSWR criterion is S and the coupling coefficient $T = Y_0/G$ (see Figure 2.2) if the antenna is modeled as a parallel resonant circuit and $T = Z_0/R$ in the series resonant case.

The bandwidth of the resonator can be increased or decreased by changing the coupling coefficient. Often, a resonator (e.g. an antenna) is perfectly matched at the resonant frequency i.e. $T = 1$ and the relative impedance bandwidth reduces from Equation (2.13) to

$$B_{r.crit} = \frac{1}{Q_0}\cdot\frac{S-1}{\sqrt{S}}, \tag{2.14}$$

where Q_0 is the unloaded quality factor of the antenna and S is the maximum VSWR at the desired frequency band. In this case the resonator is critically coupled and the input impedance curve cuts the centre of the Smith chart i.e. the losses of the resonator equal to the losses of the external circuit ($Q_e = Q_0$). The relative impedance bandwidth increases if the resonator is overcoupled. This maximum relative bandwidth $B_{r,max}$ can be found by examining the expression *(TS-1)(S-T)/S* in Equation (2.13). The coupling coefficient that leads to maximum relative bandwidth is

$$T = \frac{1}{2}\left(S + \frac{1}{S} \right). \tag{2.15}$$

The resonator is now optimally overcoupled and the relative impedance bandwidth is

$$B_{r,\max} = \frac{S^2 - 1}{2Q_0 S}. \tag{2.16}$$

If the impedance matching bandwidth must be further increased, dual-resonant or multi-resonant matching circuits can be used [7], see below.

2.3 Limitations on size reduction

Electrically small antennas have the following properties [8]:

- Low directivity
- High input reactance outside the resonance frequency and high Q_{rad}
- Low radiation efficiency

Low directivity is not a problem in mobile devices but high Q_{rad} and high input reactance are serious disadvantages. Small antennas are inefficient due to ohmic losses on the antenna structure and impedance mismatching [8]. The antenna can be tuned by using a matching circuit but as the size of the antenna decreases the matching can be done efficiently only over a narrow frequency band. That is why reduction of the size sets a fundamental limitation to bandwidth [9].

In [10] the minimum attainable radiation quality factor of a linearly polarized antenna is examined. The lower limit of the Q_{rad} is defined as

$$Q_{rad,\min} = \frac{1}{k^3 r^3} + \frac{1}{kr}, \tag{2.17}$$

where the wave number $k = 2\pi/\lambda_0$, λ_0 is the free space wavelength and r is the radius of the sphere, which encloses the antenna. It has been assumed that the antenna is lossless, except for the desired radiation losses. As it can be seen from Equation (2.17), increasing the radius r or the angular frequency ω decreases the quality factor and thereupon the achievable impedance bandwidth increases. $Q_{rad,min}$ can not be achieved with real antennas.

2.4 General matching circuit implementation methods

Antennas are not always self-resonant but they have to be tuned to resonance using e.g. a matching circuit. This tuning process is called impedance matching and it is one of the basic tasks for a radio engineer. In this section the basic methods for matching a complex load impedance $Z_L(f) = R_L(f) + jX_L(f)$ (or admittance $Y_L(f) = G_L(f) + jB_L(f)$) to 50 Ω are presented. Matching can be done using lumped elements, distributed elements, quarter-wavelength transformer or a resistive attenuator.

As long as the load impedance Z_L has some nonzero real part, matching can be done using the techniques mentioned above. However, a perfect impedance match is achieved only at a single frequency. Narrow-band matching ($B_r < 10\ \%$) can be done with one or two circuit elements. To achieve broad impedance matching bandwidth matching theory can be used to design multi-resonant matching circuits. [11]

2.4.1 SINGLE-RESONANT MATCHING WITH LUMPED ELEMENTS

Any input impedance having a finite positive resistive part can be matched using two reactive lumped elements. Lumped inductors and capacitors can be used as reactive components of a matching circuit if the length of the component is very small compared to the operating wavelength. There are two different configurations for a matching circuit (see Figure 2.5), if two reactive elements are used. Matching network elements can be defined using the Smith chart or analytic equations presented below. [6]

The reactance X and the susceptance B in Figure 2.5 (a) are [11]

$$X = \pm\sqrt{R_L\left(Z_0 - R_L\right)} - X_L \tag{2.18}$$

$$B = \pm \frac{\sqrt{(Z_0 - R_L)/R_L}}{Z_0} \tag{2.19}$$

The upper and the lower signs correspond to each other. Hence, there are two possible solutions, if $R_L \leq Z_0$. The positive X or the negative B correspond inductance and the negative X or the positive B correspond capacitance.

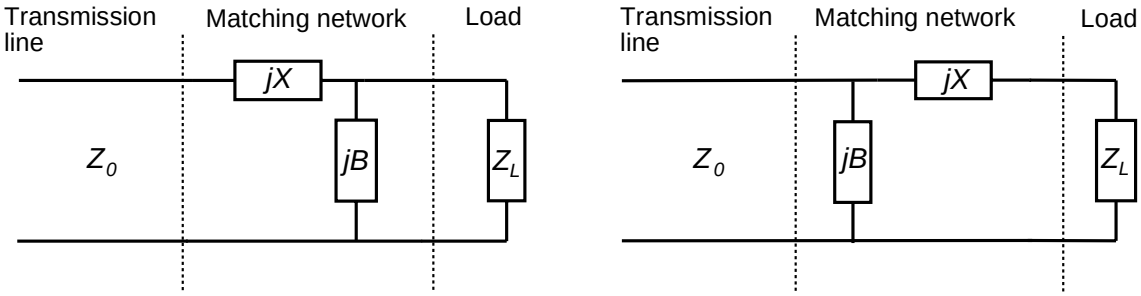

Figure 2.5: *Lumped element matching circuit topologies. X is the reactance, B is the susceptance and Z_L is the load impedance.*

In Figure 2.5 (b) the susceptance B and the reactance X are [11]

$$B = \frac{X_L \pm \sqrt{R_L/Z_0}\sqrt{R_L^2 + X_L^2 - Z_0 R_L}}{R_L^2 + X_L^2} \tag{2.20}$$

$$X = \frac{1}{B} + \frac{X_L Z_0}{R_L} - \frac{Z_0}{B R_L} \tag{2.21}$$

Again, there are two possible solutions, if $Z_0 R_L \leq R_L^2 + X_L^2$.

2.4.2 DUAL-RESONANT MATCHING WITH LUMPED ELEMENTS

The dual-resonant matching is often used in broadband antennas because the structure of the dual-resonant matching circuit is quite simple and the improvement in bandwidth compared to the single-resonant matching can be about 100 % higher (see Figure 2.4). In [12] a theoretical study on optimum dual-resonant matching circuits for small non-resonant coupling element antennas is presented. One option to implement a dual-resonant matching circuit is presented in Figure 2.6. In the figure resonator 1 consists of a capacitor C_1 and an inductor L_1 and the resonator 2 consists of a reactance X_m and an inductance L_T, which is the value of an inductor used to implement the impedance inverter-transformer. The reactance X_m is used to tune the resonator 2 into resonance and it can be either an inductor or a capacitance depending on the

non-resonant antenna impedance Z_L. The impedance inverter and transformer between the resonators can be realized with inductors or capacitors. The equations to determinate the component values are also presented in [12]. These equations work when ideal reactive component values are used. Another option to determinate component values is to use a circuit design software and an optimization tool. The Smith chart can also be utilized in the design process.

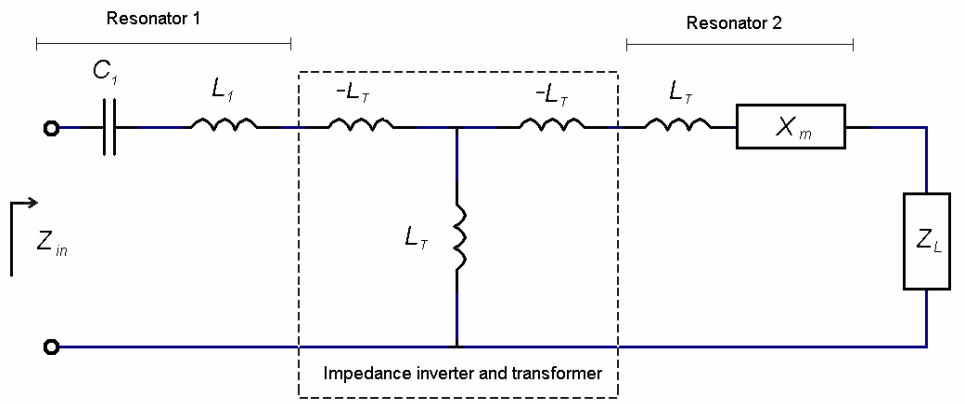

Figure 2.6: *A schematic structure of a dual-resonant matching circuit.*

The structure of the dual-resonant matching circuit used in this thesis is presented in Figure 5.9. The structure is basically the same as in Figure 2.6 but the resonator 1 is a parallel resonator instead of a series resonator. The inductance $-L_T$ between the parallel impedance inverter inductance L_T and the inductance L_1 have been included to L_1 and the inductances L_T and L_1 have then been combined.

2.4.3 MATCHING WITH DISTRIBUTED ELEMENTS

An open-ended or short-ended stub of transmission line can be used as a matching element. Especially the open-ended shunt stub is easy to fabricate in microstrip form. The single-stub shunt tuning circuit is presented in Figure 2.7.

The parameter d in Figure 2.7 is selected so that the real part of the normalized admittance $y = Y/Y_0$, seen from the transmission line is 1. The susceptance of the stub cancels the imaginary part of the admittance and the load is matched. The distance d between the load and the stub can be solved from [11]

$$\tan \beta d = \frac{X_L \pm \sqrt{R_L\left[(R_L - Z_0)^2 + X_L^2\right] / Z_0}}{R_L - Z_0}, \tag{2.22}$$

where $\beta = 2\pi/\lambda$. There are basic solutions. If $R_L = Z_0$, the solutions are $d = \lambda/4$ and $\tan \beta d = -X_L/(2Z_0)$. The susceptance of the shunt stub is [11]

$$B = \frac{(Z_0 - X_L t)(X_L + Z_0 t) - R_L^2 t}{Z_0\left[R_L^2 + (X_L + Z_0 t)^2\right]}, \tag{2.23}$$

where $t = \tan \beta d$. If the characteristic admittance of the stub is the same as the transmission line admittance Y_0, the length of the open-ended stub is [11]

$$\frac{l}{\lambda} = \frac{1}{2\pi} \arctan \frac{B}{Y_0} \tag{2.24}$$

and the length of the short-ended stub is [11]

$$\frac{l}{\lambda} = -\frac{1}{2\pi} \arctan \frac{Y_0}{B}. \tag{2.25}$$

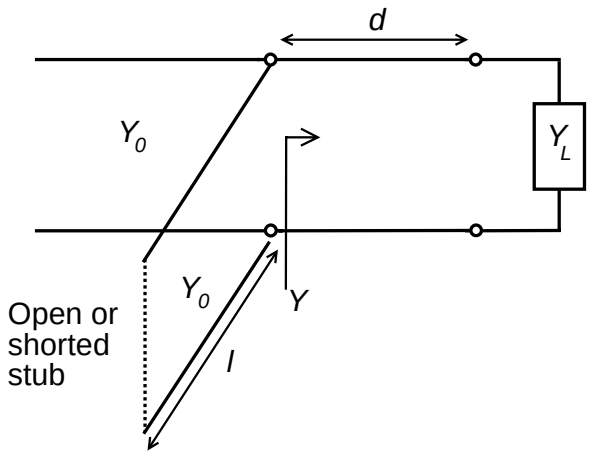

Figure 2.7: *Impedance matching using open or shortened shunt stub. l is the length of the stub, d is the distance between the load and the stub and Y_L is the load admittance.*

2.5 Directivity, efficiency and gain

Directivity is one of the radiation parameters of an antenna. It defines the ability of an antenna to focus radiation to certain direction. If the radiation pattern of the antenna is known, directivity can be calculated from [3]

$$D(\theta,\phi) = \frac{4\pi \cdot S(\theta,\phi)}{\iint_{4\pi} S(\theta,\phi) \cdot \sin(\theta) d\theta d\phi}. \tag{2.26}$$

In the equation $S(\theta,\phi)$ is power density, θ is the elevation angle and ϕ is the azimuth angle in the standard spherical coordinate system (see Figure 2.8).

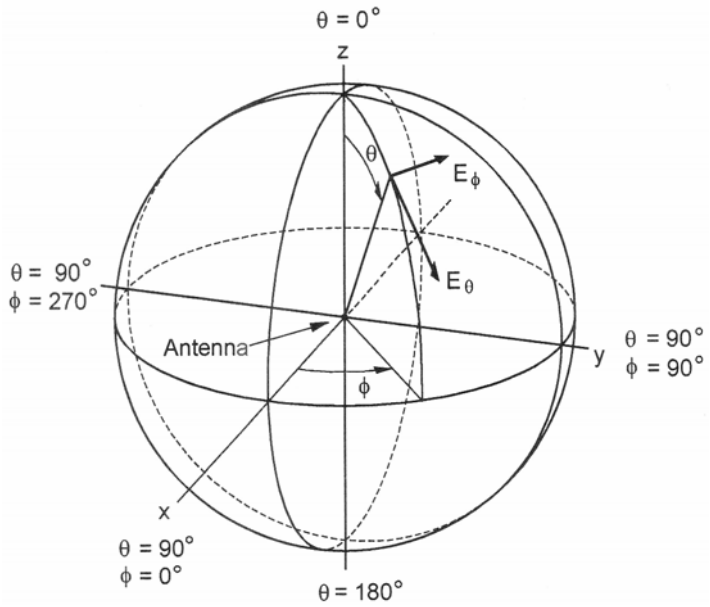

Figure 2.8: *The standard spherical coordinate system [3].*

Antenna efficiency gives information about different loss mechanisms in the antenna. The total antenna efficiency η_{tot} takes into account both losses due mismatching in feed network and the losses within the antenna structure. It can be defined as a ratio between the radiated power P_{rad} and the total incident power P_t [13]

$$\eta_{tot} = \frac{P_{rad}}{P_t} = \eta_m \eta_{rad}. \tag{2.27}$$

As can be seen from (2.27) the total antenna efficiency can be divided into matching efficiency η_m and radiation efficiency η_{rad}. The matching efficiency is the ratio between the power accepted

by the antenna P_{in} and the total incident power P_t. It can also be calculated from the voltage reflection coefficient (in Equation (2.1)) as follows

$$\eta_m = \frac{P_{in}}{P_t} = 1 - |\rho|^2 . \tag{2.28}$$

The radiation efficiency η_{rad} is defined as the ratio between the powers radiated and accepted by the antenna

$$\eta_{rad} = \frac{P_{rad}}{P_{in}} . \tag{2.29}$$

If the antenna structure is lossless, all the power accepted by the antenna is radiated and the radiation efficiency is 1.

The gain of the antenna is the ratio of the power density, in a given direction, to the power density obtained if the power accepted by the antenna would be radiated isotropically. If there are no losses in the antenna structure the gain is equal to the directivity. The gain can be expressed with the directivity D and the radiation efficiency η_{rad} as [13]

$$G = \eta_{rad} D . \tag{2.30}$$

The gain does not include losses due to mismatching and that is why it is useful to define realized gain G_r as

$$G_r = \eta_{tot} D . \tag{2.31}$$

2.6 Compact coupling element based antenna structure

Until now, the resonator theory and impedance matching strategies have been discussed. However, an antenna can be implemented also with a non-resonant antenna element (later referred to as a coupling element) and a solid metal plane. The coupling element antenna is tuned to resonance with a matching circuit and the same quality factors and impedance matching strategies can be used to optimize the operation of the antenna.

A non-resonant compact coupling element structure has been studied in [14]. In a mobile terminal the printed circuit board and EMC shielding often form a solid metal plane which is called a ground plane in this work. The ground plane can be used as a part of the antenna structure. At low frequencies (below 1 GHz) the antenna element works mainly as a nonradiating coupling element and the ground plane operates as the main radiator [15]. The

main advantages of the coupling element antenna are low volume and flexibility of design. A resonance can be tuned to a desired frequency using a matching circuit between the feed and the coupling element. Also multi-resonant matching circuits can be used to obtain a broader bandwidth. The mechanical structure of the coupling element antenna is not strictly defined because the antenna element is not in resonance.

The ground plane radiates like a thick dipole because it has the same kind of current distribution. The currents in the ground plane are induced capacitively via electric fields. The lowest quality factor and the largest bandwidth are achieved when the ground plane is at resonance. In [15] it has been found out that for a ground plane with length 80 – 130 mm and width 40 mm the first order resonance *λ/2* is approximately

$$f_{rc} = (0.73...0.78) \cdot \frac{c}{2l}. \tag{2.32}$$

Here c is the speed of light and l is the length of the ground plane. The quality factor of the ground plane resonance is so low (below 5) that it is difficult to define the resonance frequency f_{rc} exactly.

The optimum location for the coupling element has been studied in [14] and [16]. The strongest coupling to the ground plane is achieved when the coupling element is placed on the short side of the ground plane (as in Figure 4.4) or in the corners where the electric fields are at the maximum. Coupling can be further increased by bending the coupling element over the edge. Stronger coupling leads also to broader achievable bandwidth if the size of the ground plane is the same.

3 MULTI-ELEMENT ANTENNA SYSTEMS

The goal of this thesis is to gain knowledge on the feasibility of multi-element antenna solutions for a mobile DVB-H terminal. Multi-element antennas can be used in mobile communications to improve transmission rate or reliability of wireless communication. The performance improvements are due to array gain, diversity gain, spatial multiplexing gain and interference reduction [17]. In this thesis, only diversity and spatial multiplexing techniques are discussed. At the end of the chapter a few multi-element antenna structures are presented.

3.1 Applications of multi-element antenna systems

A multiple-input single-output (MISO) system uses multi-element antennas in a receiver (Rx) and a single-input multiple-output (MISO) system uses them in a transmitter (Tx). In MISO and SIMO systems diversity can be used to prevent the signal blackouts caused by fast fading. A MIMO system utilizes several antennas in Tx and Rx (Figure 3.1) and it transmits data over a channel matrix (see Eq. 3.2) rather than just over a single radio channel. The channel matrix represents the transmission at a certain time, spatial locations of the antennas and directions of the radiation beams. The transferred signal is combined at both Tx and Rx ends so that the quality of the link in terms of the bit-error rate can be improved [18]. This requires signal processing over space and time. Also in a MIMO system diversity can be used to increase SNR in fading dips. In addition, MIMO can exploit spatial multiplexing to significantly increase the mutual information. The drawback of using a multi-element antenna system is the increased transceiver complexity.

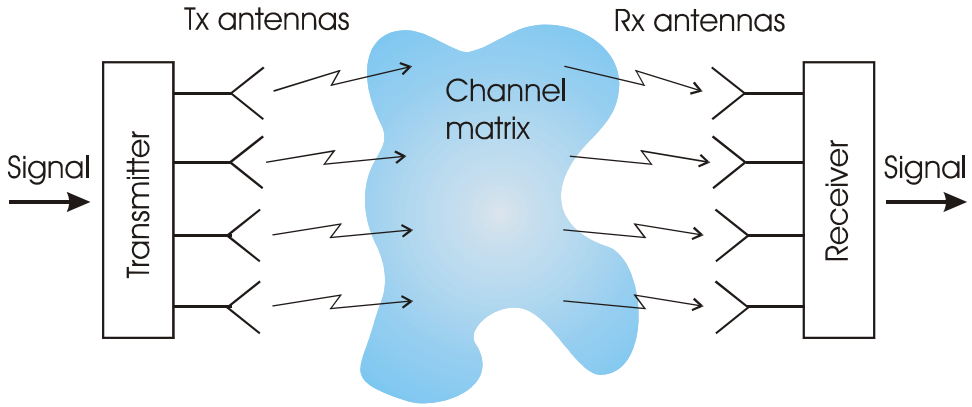

Figure 3.1: *Illustration of a MIMO system with four Tx and four Rx antennas.*

3.1.1 DIVERSITY AND ENVELOPE CORRELATION COEFFICIENT

Signal amplitude level fluctuates randomly in a wireless propagation channel. This fluctuation is called fading and it can be a serious problem especially in non-line-of-sight (NLOS) propagation environments. Diversity technique in telecommunications means that several independent copies of the signal are obtained and the best combination of the signals is chosen according to a diversity technique used. This increases the SNR in fading dips. Diversity is a powerful tool to reduce fading in radio links. The copies of the signal can be separated in time, frequency or space. [17]

To evaluate the diversity performance of the antenna system, diversity gain and envelope correlation coefficient can be defined. The diversity gain is a relative time averaged measure of the signal-to-noise ratio improvement of the system achieved by combining the signals received by at least two antennas as compared to the signal from the best performing antenna of the same system. The diversity gain is assumed for a certain probability level, e.g. 50 % or 90 % and it is depended on correlation of the signals and power balance between diversity branches. The lower the correlation and the power imbalance are the higher the achievable diversity gain will be. The envelope correlation coefficient ρ_e can be used to estimate the achievable diversity gain of the antenna system. To provide a sufficient diversity gain a commonly used upper boundary for the envelope correlation coefficient is 0.7 [19]. The envelope correlation coefficient between two antennas, in a Rayleigh fading environment is given by [20]

$$\rho_e = \frac{\left| \int_\Omega \left[E_{1\theta} E_{2\theta}^* p_\theta + X E_{1\phi} E_{2\phi}^* p_\phi \right] \right|^2}{\int_\Omega \left[E_{1\theta} E_{1\theta}^* p_\theta + X E_{1\phi} E_{1\phi}^* p_\phi \right] d\Omega \int_\Omega \left[E_{2\theta} E_{2\theta}^* p_\theta + X E_{2\phi} E_{2\phi}^* p_\phi \right] d\Omega}, \tag{3.1}$$

where E_θ and E_ϕ are the θ and ϕ polarized complex electric field patterns of the evaluated antennas, respectively, X is the cross-polar ratio P_ϕ / P_θ where P_θ and P_ϕ are the powers that would be received by isotropic θ- and ϕ-polarized antennas, respectively, in a multipath environment, and p_θ and p_ϕ are the angular power distribution functions of the incoming θ- and ϕ-polarized plane waves, respectively.

In mobile terminals antennas are close to each other. If the distance between the antennas is less than a quarter wavelength, it is difficult to obtain two uncorrelated signals. However, it is possible (see Section 6.4). Polarization diversity and beam pattern diversity are the most promising techniques to do this especially at low frequencies.

3.1.2 SPATIAL MULTIPLEXING

Spatial multiplexing is a MIMO transmission technique to transmit independent data signals from multiple Tx antennas at the same time. At first the signal is encoded, modulated and mapped in Tx. Then different signals are transmitted simultaneously from the TX antenna elements. At Rx each antenna element receives a signal from each Tx antenna element. If the signals are sufficiently independent the original transmitted signal can be re-established. Because of that, in theory a MIMO system with *n* antennas in the transmitter and the receiver and spatial multiplexing can multiply the potential mutual information by a factor *n* compared to a single element antenna system. In the real world only 40 – 60 % of the ideal potential mutual information can be achieved with MIMO because the ideal case would require an ideal multipath channel and totally uncorrelated signals in the receiver [21]. The basic differences between diversity and spatial multiplexing can be described as follows. When diversity is used only one signal is transmitted at a time but in spatial multiplexing multiple signals are transmitted simultaneously. Diversity system does not necessarily require multiple antennas in both Tx and Rx ends. Diversity is usually utilized to increase SNR at fading dips whereas spatial multiplexing is normally used to increase the mutual information of a MIMO system.

In this thesis the MIMO performance of the multi-element antenna is evaluated with MEBAT [22]. Introduction to MEBAT is presented in Section 7.1 but the equations that are used in MEBAT simulation to calculate the figure of merits in MIMO analysis are presented in this section. The following equations have been selected so that they can be utilized in the MEBAT simulations.

The received signal of the MIMO system can be defined as a vector $\mathbf{y}(t) = \mathbf{H}(t)\mathbf{s}(t) + \mathbf{n}(t)$, where $\mathbf{H}(t)$ is the channel matrix, $\mathbf{s}(t)$ is transmitted signal vector and $\mathbf{n}(t)$ represents the noise vector which is assumed to be complex Gaussian variables. The complex narrowband channel matrix can be denoted in matrix form by

$$\mathbf{H}(t) = \begin{bmatrix} h(t)_{1,1} & \cdots & h(t)_{1,n_r} \\ \vdots & \ddots & \vdots \\ h(t)_{n_t,1} & \cdots & h(t)_{n_t,n_r} \end{bmatrix}, \tag{3.2}$$

where $h(t)_{i.j}$ represents the transmission coefficient from Tx antenna *i* to Rx antenna *j* at certain time *t*. The mutual information of the MIMO system is defined as [23]

$$I_H^{(i)} = \log_2 \left| \mathbf{I} + \frac{\rho}{n_t} \mathbf{H}(t)\mathbf{H}(t)^H \right| \text{ [bit/s/Hz]}, \tag{3.3}$$

where $|\bullet|$ detonates a determinant, $(\bullet)^H$ stands for complex conjugate or Hermitian transpose, n_t is the number of Tx antennas, **I** is identity matrix and ρ is the SNR at the input of each receiving antennas. The expression $\mathbf{H}(t)\mathbf{H}(t)^H$ can be called the channel correlation matrix. In expression (3.3) the total transmitted power is divided equally to all Tx antennas and the channel matrix is assumed to be known at the receiver but unknown at the transmitter.

As can be seen from (3.3) the performance of the MIMO system is defined by the channel matrix $\mathbf{H}(t)$. The singular values of $\mathbf{H}(t)$ or the eigenvalues of the channel correlation matrix $\mathbf{H}(t)\mathbf{H}(t)^H$ give information about the parallel independent propagation channels that can be exploited in a MIMO system. The number of eigenvalues is defined by the minimum number of n_t and n_r. In a rich scattering environment eigenvalue spread is low and a good MIMO performance can be achieved. In [21] the mutual information of a MIMO system has been divided to transferred signal power (3.4) and to the system's ability to use parallel spatial channels (spatial multiplexing efficiency (3.5)). The equations presented below are derived in [21].

Transferred signal power is defined in [21] and [24] as.

$$G_{ant}^{(i)} = \frac{\left\| \mathbf{H}_{ant}^{(i)} \right\|_F^2}{\left\| \mathbf{H}_{ref,sli}^{(i)} \right\|_F^2}, \tag{3.4}$$

where $\mathbf{H}_{ant}^{(i)}$ is the measured channel matrix of the antenna under test, $\mathbf{H}_{ref,sli}^{(i)}$ is a sliding mean over the samples of the channel matrix of the reference antenna and $\|\bullet\|_F$ denotes a Frobenius form of the matrix. Transferred signal power (3.4) is defined so that it is not depended on the number of antennas. In the MEBAT simulations an ideal dual polarized isotropic antenna was used as a reference antenna. The ideal isotropic reference antenna receives signal evenly from every direction and adapts to all polarizations of each incoming wave perfectly and that is why the absolute values of the MEBAT simulation result are so low.

Spatial multiplexing efficiency can be expressed as [21]

$$G_{mux}^{(i)} = \frac{m_g^{(i)}}{m_a^{(i)}} = \frac{\left(\prod_{k=1}^{K} \lambda_k^{(i)} \right)^{1/K}}{\frac{1}{K} \sum_{k=1}^{K} \lambda_k^{(i)}}, \tag{3.5}$$

which is a ratio of geometric and arithmetic means of the eigenvalues $\lambda_k^{(i)}$ of the channel correlation matrix $\mathbf{H}(t)\mathbf{H}(t)^H$.

3.2 Multi-element antenna designs

According to literary research multi-element configurations for DVB-H have not been reported. Before DVB-H most system standards at low frequencies (e.g. GSM 900) have not included multi-element antennas at the mobile end and that is why only small amount of publications or commercial products have been presented about the subject. However, due to need of high mutual information MIMO could be included in the DVB-H standard in the future if feasible multi-element antennas could be developed.

In [25] the diversity performance of three dual-antenna solutions for a traditional handset has been evaluated at 902-928 MHz. The evaluated antenna configurations are presented in Figure 3.2. The evaluation criterion of the antenna configurations is the power correlation coefficient ρ_p which has been measured along four different indoor routes. As said in the paper, the power correlation ρ_p and the envelope correlation ρ_e (3.1) correspond to each other for all practical purposes. Measured correlation coefficients are under 0.2 with all antenna configurations and the best performing option seems to be the one with two side-mounted PIFA's (Figure 3.2 (a)). The correlation coefficients of the antenna configurations (a-c) in Figure 3.2 are approximately equal to correlation of two vertically oriented dipoles with 0.4λ horizontal separation. The bandwidth of the antennas is quite narrow (B_r = 2.8 % at VSWR ≤ 2) which can partly explain the low correlation of the antennas. [25]

When the frequency gets higher it is easier to implement uncorrelated antennas for small devices. At about 2 GHz many realistic multi-element antennas have been presented for modern mobile terminals. One of the multi-antenna studies for the UMTS system is presented in [26]. The antenna configurations (A1-A4) used in [26] are shown in Figure 3.3. All these antennas cover the UMTS frequency band (1900 – 2170 MHz, B_r = 13 %) with impedance matching criterion $S_{11} \leq$ -6 dB. The first three configurations (A1-A3) are implemented with traditional square-shaped PIFAs but the antenna configuration A4 comprises of a multi-band (E-GSM900, GSM1800 and GSM1900) PIFA and an IFA (inverted F-antenna) at the same end of the ground plane. All these antenna configurations have quite equal envelope correlation coefficient ρ_e from 0.41 to 0.43. The MIMO performance of the antennas has been evaluated with MEBAT simulations. The highest average mutual information is achieved with A1 (4.2 bits/s/Hz) and the lowest with A2 (3.1 bits/s/Hz). The average mutual informations of A3 and A4 are 3.2 bits/s/Hz and 3.3 bits/s/Hz, respectively. [26]

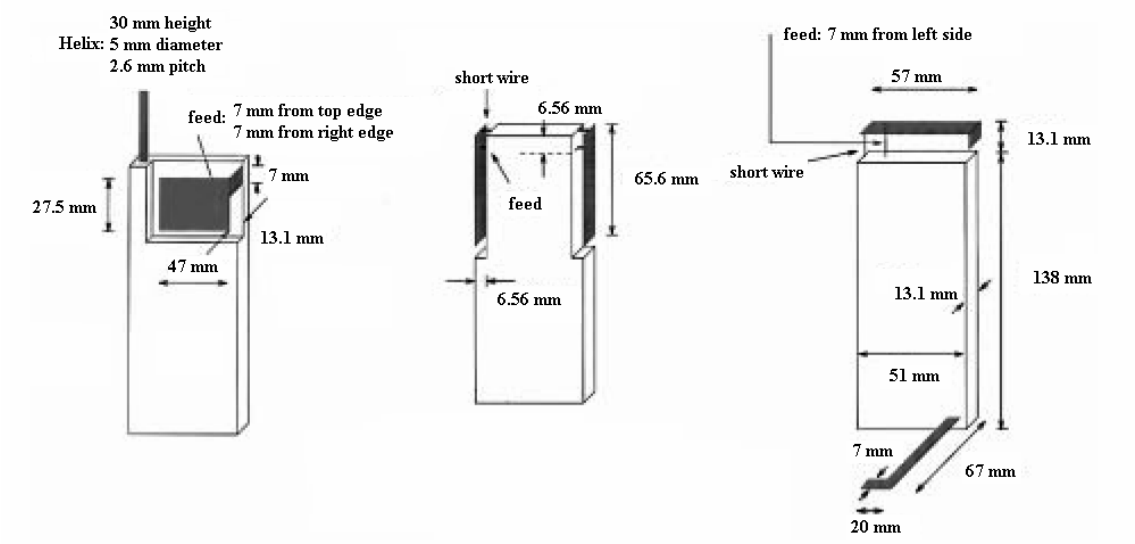

Figure 3.2: *The antenna configurations presented in [25]: (a) a top mounted helix and a back-mounted PIFA, (b) two side-mounted PIFA's and (c) a top mounted PIFA and a "flip" monopole.*

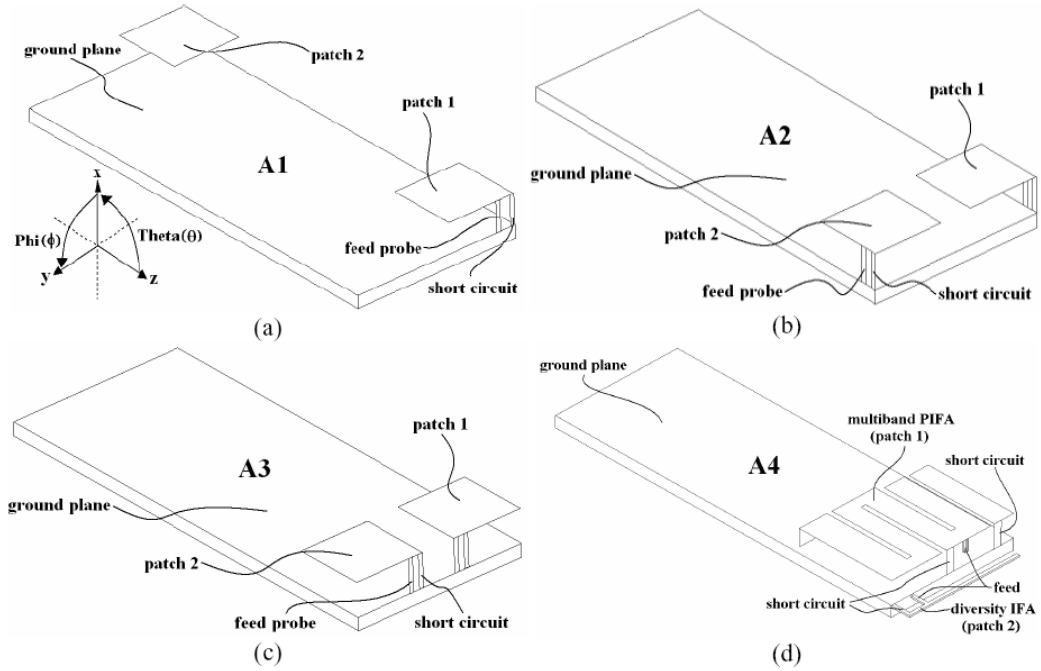

Figure 3.3: *The designed antenna geometries (a) A1, (b) A2, (c) A3 and (d) A4 in [26].*

4 DIGITAL TELEVISION IN HANDHELD DEVICES

Several standards like DVB-H, DMB, 1seg, TDtv and MediaFLO have been developed to bring the digital TV to handheld devices. These standards can be divided to two groups according to the data transport mechanism. One alternative is to use a cellular network to data transmission (e.g. TDtv). While providing flexibility of content, this technique is generally unsuitable for high-quality mobile DTV transmissions due to bandwidth and capacity limitations of the cellular network. Another option is broadband transmission (e.g. DVB-H, DMB, 1seg and MediaFLO), which is a unidirectional service and suitable for high quality DTV streaming transmissions. The same data is sent to all users and desired content is separated by choosing a right channel. The division of the standards can also be done geographically since DVB-H is mainly promoted in Europe and the US, MediaFLO in the US, DMB in Korea and 1seg in Japan [27]. In this thesis we focus on the DVB-H technology.

The Digital Video Broadcasting Project was launched in 1993 and consists of about 300 companies worldwide. Its objective is to agree on specifications for digital media delivery systems. The specifications are then standardised by international standards' organizations such as European Committee for Electrotechnical Standardization (CENELEC) or European Telecommunications Standards Institute (ETSI). Services using DVB standards are adopted and launched currently in over 30 countries all over the world and the number is increasing constantly. [28]

In this chapter technology behind the DVB-H system is presented. First in Section 4.1 the DVB-H standard is presented. In Section 4.2 the antenna performance requirements for DVB-H are presented and in Section 4.3 the possible antenna solutions for DVB-H terminals are introduced.

4.1 DVB-H system

DVB-H is a standard for the delivery of IP based media content and data to handheld receivers. The main purpose of DVB-H is to bring digital television to handheld devices. It is an efficient way to broadcast data for several users. DVB-H is an approved standard since November 2004 for handheld devices by ETSI. It has been developed from DVB-T (terrestrial) standard to meet the special needs of a mobile receiver. Other DVB systems are DVB-C (cable) and DVB-S (satellite) [28].

DVB-H is based on DVB-T, but operating in the IP environment and with several special features for mobile receiving. A block diagram of a DVB-H receiver is presented in Figure 4.1. Time slicing is a technique to reduce the power consumption of a receiver. The received signal is divided in bursts and the receiver is active only a fraction of the time. This reduces the average power consumption in the receiver up to about 90 – 95 %. In addition, Time slicing enables smooth and seamless service handover. Forward error correction for multiprotocol encapsulated data (MPE-FEC) has been added to DVB-H to improve signal-to-noise ratio (SNR) and Doppler performance in mobile channels and to improve tolerance to impulse interference. This is done by adding parity information calculated from the datagrams and sending this parity data in separate MPE-FEC sections. [29]

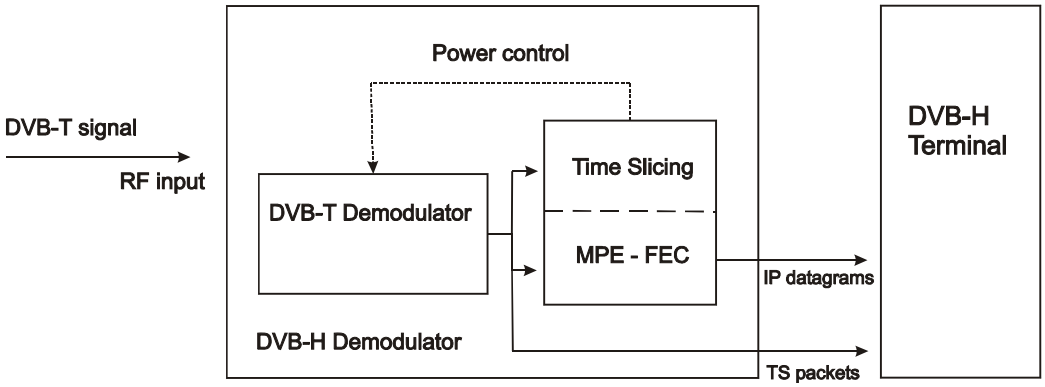

Figure 4.1: *A block diagram of a DVB-H receiver.*

4.2 Performance requirements for a DVB-H antenna

DVB-H operates in the frequency band 470 – 858 MHz. In practice, the higher part of the band is not typically in use. The DVB-H band is usually limited to 470 – 700 MHz because the isolation between DVB-H and GSM 900 is low [30]. GSM signal leaks to the sensitive DVB-H receiver and disturbs the operation of the receiver. If the DVB-H band is limited to 700 MHz the relative bandwidth (see 2.16) B_r = 40 %. The free space wavelength λ_0 at the center frequency 586 MHz is 0.512 m. Therefore the antenna inside a handheld terminal will be small compared to the wavelength. The resistive part of the antenna impedance is small due to the small size of the antenna and achieving sufficient impedance matching at the whole frequency range is a difficult task. Poor impedance matching leads to high losses and to low total antenna efficiency. The total antenna efficiency is defined as a product of matching efficiency and radiation efficiency. Because a DVB-H antenna operates only as a receiving antenna reflections from the impedance mismatch may be tolerated as far as SNR is high enough. For transmitter

antennas the impedance matching and the total antenna efficiency are the main design criteria purposes because reflections from the antenna can lead to high power consumption and heat producing. The main design parameter for DVB-H antenna is realized gain which is defined as a product of radiation efficiency, matching efficiency and directivity. The realized gain specification, typically used for internal handheld terminal DVB-H antennas, is presented in Figure 4.2 [31]. The specification begins from -10 dBi at 474 MHz and increases linearly to -7dBi at 698 MHz and to -5 dBi at 858 MHz. The specification has been given for an antenna inside a real handheld terminal where plastic covers and other lossy parts deteriorate the gain of the antenna. This is why a few decibel margin to the specification is needed when designing antenna prototypes without other parts of the terminal. The impedance matching criterion is not specified but normally the absolute value of the voltage reflection coefficient is below -1.5 dB.

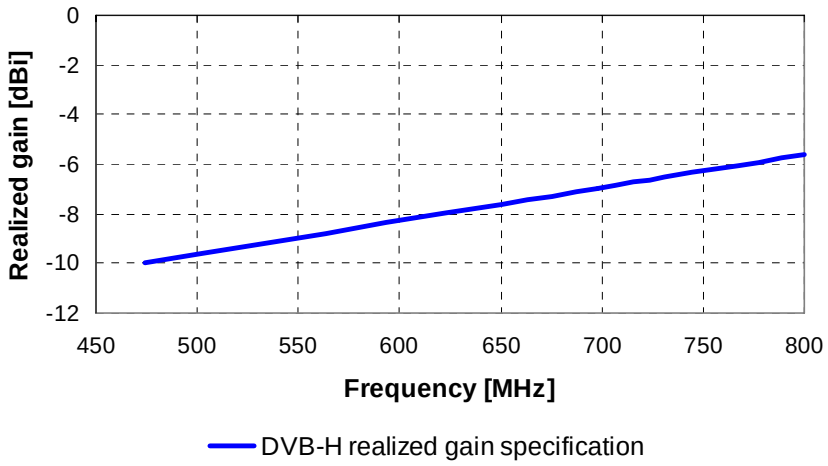

Figure 4.2: *The realized gain specification for DVB-H antenna.*

Also the influence of the user on the radiation characteristics of the antenna has to be taken into consideration. The presence of the human body affects the radiation pattern of the antenna and decreases the total antenna efficiency [32]. The Specific Absorption Rate (SAR) is an insignificant quantity because a DVB-H terminal acts only as a receiver.

4.3 Possible antenna solutions for a DVB-H terminal

DVB-H is a relatively new technology and that's why there are quite small amount of antenna solutions for DVB-H terminals. In this work we consider only internal antennas that would be suitable for handheld terminals. A planar spiral antenna and a bow-tie antenna in Figure 4.3 are broadband internal antennas. The structure of the spiral antenna is self-complementary, which

means that the shape of its complementary structure is exactly identical with the original structure. Self-complementary antennas have a wide impedance bandwidth because their input impedance is independent of the frequency. The spiral antenna in Figure 4.3 (a) consists of two metallic strips that form a spiral pattern. The feed of the antenna is in the middle. The radius of the antenna *r* is determined by the lower limit of a frequency band. At 470 MHz the wavelength is about 640 mm and the radius is roughly a quarter wavelength. Hence, the diameter of the antenna is more than 300 mm, which is too much for a mobile terminal. Other drawback is that a solid metal ground plane of a mobile terminal disturbs the radiation of a spiral antenna and lowers the achievable bandwidth [8]. A bow-tie antenna in Figure 4.3 (b) is a planar version of a finite biconical antenna and it consists of two metallic triangles with corners against each other. The radiation pattern resembles the pattern of a dipole and the antenna is linearly polarized. The feed is in the middle of the antenna between the corners. This structure is also too large for a handheld DVB-H terminal since the radius of the antenna *r* must be at least a quarter wavelength. A solid metal plane near the antenna disturbs also the radiation of a bow-tie antenna [8].

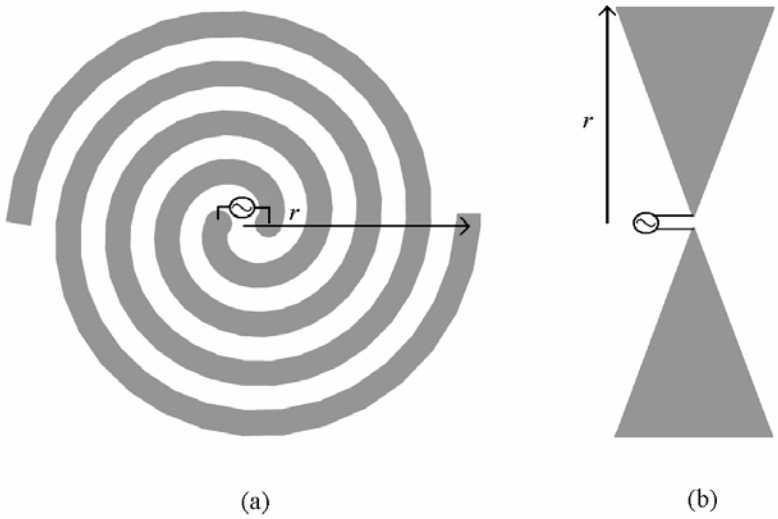

Figure 4.3: *The structure of (a) a spiral antenna and (b) a bow-tie antenna.*

Microstrip antennas are widely used in mobile phones because they are easy to implement, relatively cheap and have a compact structure. The problem of these antennas is also large size at low operating frequencies. The antenna has to be in resonance and the sum of the dimensions has to be a quarter-wave. In addition, the bandwidth of the microstrip antennas is quite narrow.

One alternative is to use a coupling element antenna described in section 2.6. They provide low volume and designing flexibility. A compact coupling element based antenna structure for

DVB-H terminal is presented in [33]. The antenna structure in [33] (see Figure 4.4) is optimized and the realized gain specification (see Figure 4.2) is fulfilled with a 3.5 dB margin by using one fixed dual-resonant matching circuit. The ground plane dimensions are 130 mm x 75 mm (length x width) and the volume of the coupling element is 1.5 cm^3.

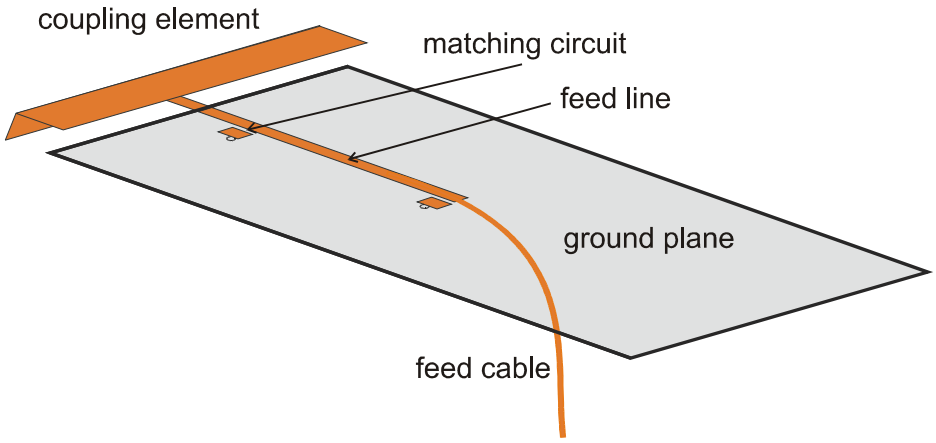

Figure 4.4: *A compact coupling element based antenna for DVB-H receiving [33].*

Pulse Finland Oy (previously known as LK Products Oy) has introduced a commercial DVB-H antenna (see Figure 4.5) based on the compact coupling element structure. The dimensions of the antenna are 45 x 7 x 6 mm^3 (w x l x h) and it is meant to be mounted on the edge of a circuit board. The volume of the coupling element is 1.9 cm^3. The matching network is integrated to the antenna element. This antenna fulfils the DVB-H realized gain specification (see Figure 4.2) with 1 dB margin at a frequency range f = 470 – 750 MHz when the size of the ground plane is 100 x 45 mm^2. [34]

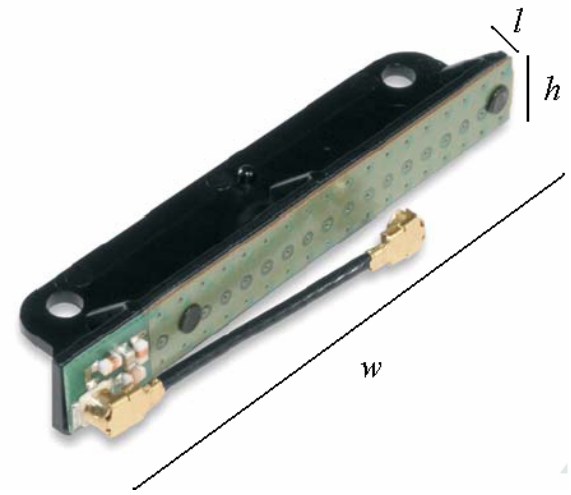

Figure 4.5: *A commercial DVB-H antenna manufactured by Pulse Finland Oy [34].*

Direct coupling is a new approach of implementing a DVB-H antenna. Direct coupling means that the power is coupled directly to the ground plane over an impedance discontinuity, which can be formed by a slot in the ground plane. The structure of the antenna is presented in Figure 4.6 [35]. The best place for the feed would be in the middle of the ground plane because currents are strongest there. However, in [35] the middle part of the ground plane is reserved for a display. The right slot is used to feed currents to the ground plane and the left slot is formed in order to lengthen the path of the current and decrease the first order resonant frequency of the ground plane. The resonance is further tuned by using a single-resonant matching circuit. The antenna fulfils the DVB-H realized gain specification with a 4 dB margin at 470 – 700 MHz [35]. The volume of the antenna is almost zero because no antenna element is needed. However, the matching circuit elements use some area from circuit board. One drawback of this antenna is that any conducting parts cannot be placed over a slot because it prevents the operation of the antenna. This is why the volume over the slots could be considered as volume reserved by the antenna.

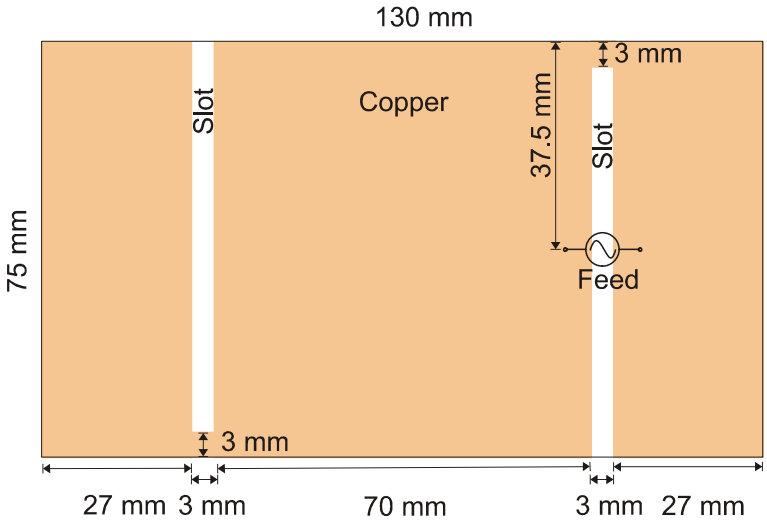

Figure 4.6: *DVB-H antenna using direct coupling [35].*

5 DESIGN PROCESS OF A MULTI-ELEMENT DVB-H ANTENNA

In this work the multi-element antenna structure is based on compact coupling elements. Coupling elements were chosen because they allow impedance tuning using matching circuits and the shape of the coupling elements is not restricted because the antenna element is not in resonance. It has been noticed that the smallest possible antenna element can be realized with coupling element antenna structure. The selection depended also on the fact that there exists a commercial DVB-H antenna based on coupling elements [34]. In Figure 5.1 the possible locations for the DVB-H antennas are presented. As can be seen from the figure the ends of the mobile terminal chassis are reserved for a cellular antenna and connectors. The possible DVB-H antenna locations are on the sides of the chassis. The corners of the chassis are good places for coupling elements because coupling to the ground plane wavemode is strong [14].

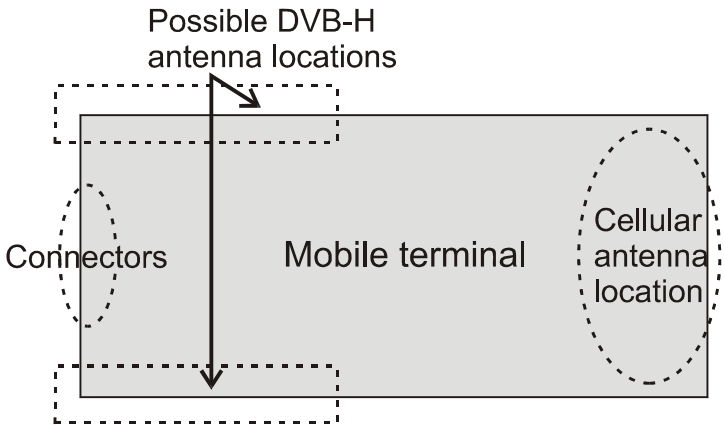

Figure 5.1: *Possible locations for DVB-H antenna.*

5.1 Simulations with IE3D

At first, several possible antenna structures were tested with simulations. The used simulation program was IE3D. It is an electromagnetic simulator based on the method of moments (MOM). The simulation model was designed to fulfil the mechanical restrictions that were given. The first restriction was the locations of the antenna elements (see Figure 5.1). The maximum dimensions of the ground plane had to be length 110 mm and width 55 mm which is the size of a typical mobile terminal. The maximum allowed height of the antenna (*h* in Figure 5.2) was defined to be 5 mm.

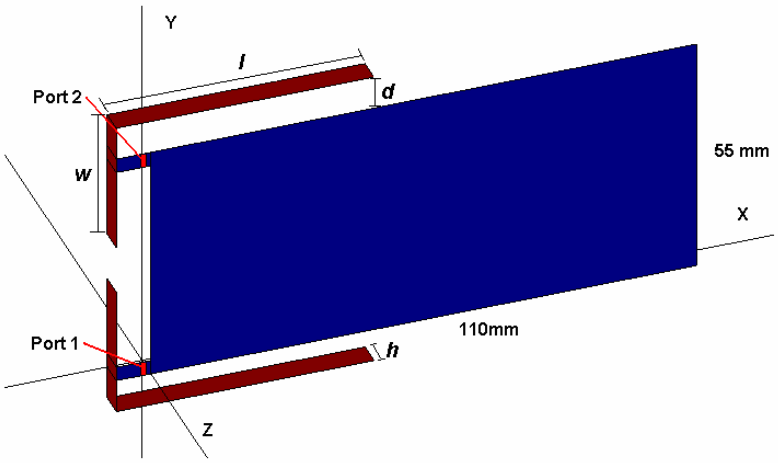

Figure 5.2: *The structure and the dimensions of the simulated antenna.*

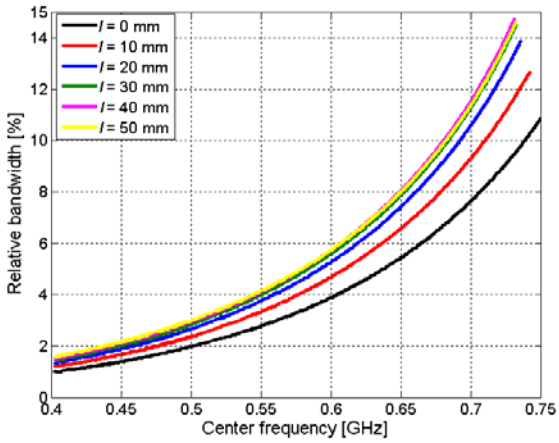

(a) achievable bandwidths with different lengths *l*

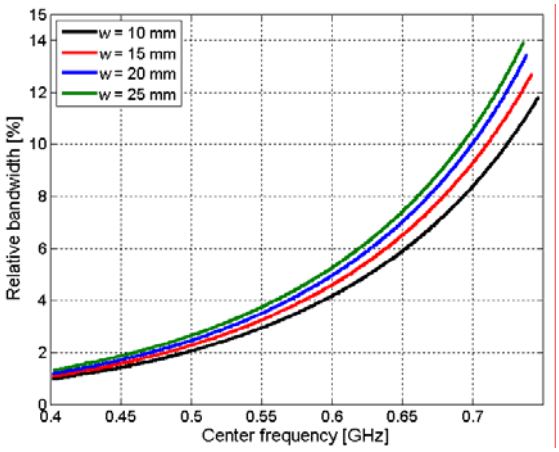

(b) achievable bandwidths with different wides *w*

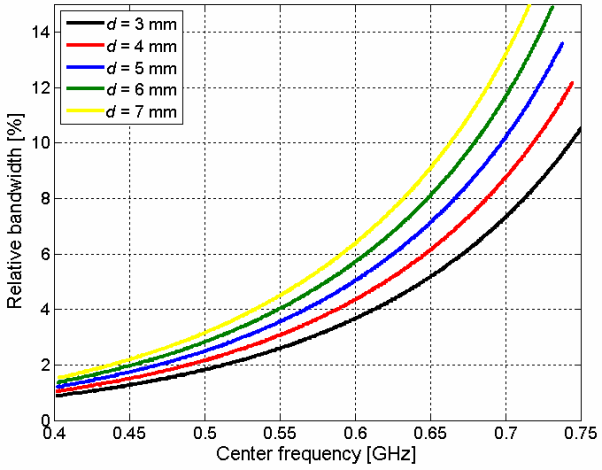

(c) achievable bandwidths with different distances *d*

Figure 5.3: *Achievable bandwidths with 2 dB return loss as a function of the center frequency. The dimensions of the antenna are l = 20 mm, w = 25 mm, d = 5 mm and h = 5 mm when they are not set as optimization variable.*

The first promising design is presented in Figure 5.2. The envelope correlation (Equation 3.1) of the radiation patterns was under 0.7 at the whole DVB-H band and it seemed that the realized gain specification (see Figure 4.2) can also be fulfilled. The dimensions of the antenna were l = 52 mm, w = 27 mm, d = 7 mm and h = 5 mm.

However, the first design was too large for a mobile terminal. The dimensions of the antenna were reduced and the effect on the achievable bandwidth of the antenna was estimated with Matlab simulations. The simulation results are presented in Figure 5.3. Critical coupling and 2 dB return loss were assumed in the simulations. From Figure 5.3 (a and b) it can be seen that the increase in length l or width w does not increase the achievable bandwidth significantly after 20 mm. The distance of the antenna element d increases the bandwidth quite evenly.

5.2 Prototype antenna

After simulations a prototype was built to test the antenna with measurements. The dimensions that were chosen to the prototype antenna are shown in Figure 5.4. The dimensions of the antenna were chosen so that it would fit inside a typical mobile phone and still have sufficient bandwidth at DVB-H frequency band. Two metal planes were added on the top of the coupling elements in order to increase the achievable bandwidth.

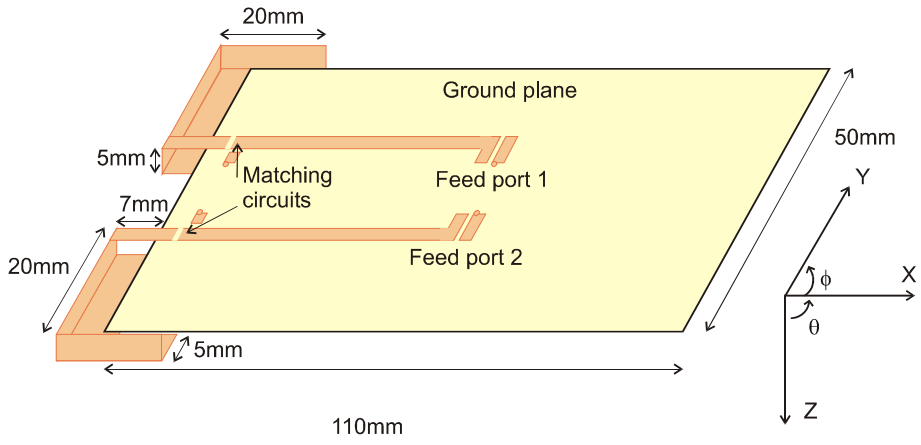

Figure 5.4: *The structure and the dimensions of the dual-element prototype antenna.*

The prototype was built at the Radio Laboratory of Helsinki University of Technology (TKK) and the circuit board was manufactured at the printed circuit board fabrication workshop of TKK. The used two-sided printed circuit board (PCB) was RT Duroid 5870 having the following properties: ε_r = 2.33, h = 0.79 mm, tan δ = 0.0012 and σ = 5.7×10^7 S/m. Since the backside of the circuit board was left metal-coated, it can be used as a ground plane and the feed

strips act as microstrip lines. The basic idea of the coupling element antenna is that the antenna element couples currents capacitively via electric fields to the ground plane and the antenna does not work without the ground plane. Four through copperized holes were made for the outer conductors of the coaxial feed cables and the parallel inductors. The coupling elements were made and soldered to the PCB. A piece of styrofoam was placed between the coupling element and the ground plane to support the structure. Pieces of Kapton tape were used to attach the coupling elements and the styrofoam. The electrical properties of styrofoam and Kapton tape are very close to air and they are almost invisible at radio frequencies. Two photographs of the prototype are shown in Figure 5.5 and Figure 5.6.

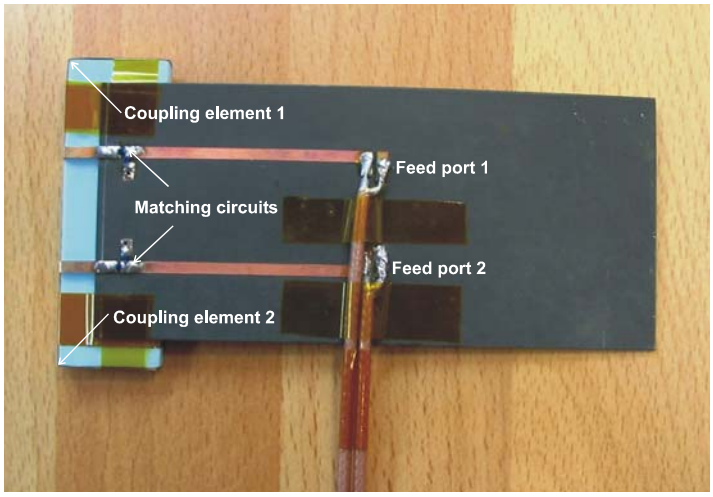

Figure 5.5: *The dual-element prototype antenna.*

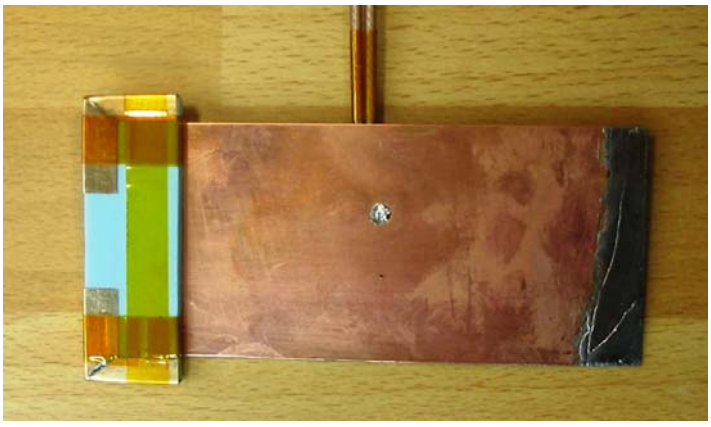

Figure 5.6: *The backside of the prototype antenna.*

5.3 Matching circuit design for the prototype antenna

The operating frequency of the prototype antenna can be tuned by selecting a proper matching circuit for the antenna. The impedance curve of the prototype antenna without the matching circuit is presented in Figure 5.7. The real and the imaginary part of the impedance are high at the simulated frequency band. The imaginary part is negative which means that the antenna can be considered as a capacitive load impedance. The impedance of the two coupling elements is equal because the structure of the antenna is symmetric. In the following sections three different matching circuits are presented: a single-resonant matching circuit and two dual-resonant matching circuits with ideal and real matching components.

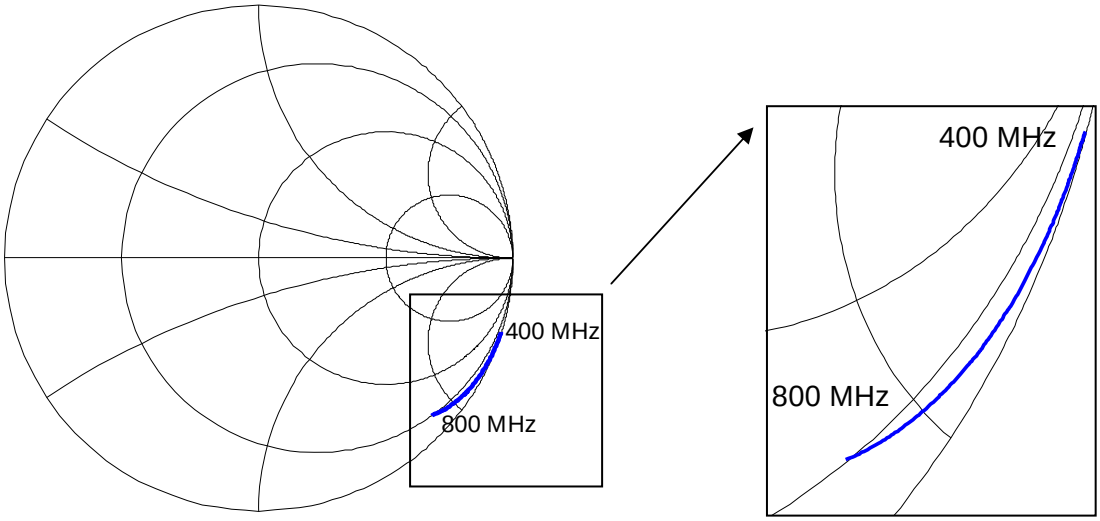

Figure 5.7: *The input impedance of the prototype antenna*

5.3.1 SINGLE-RESONANT MATCHING

The prototype antenna was measured within an international radio channel measurement campaign. These measurements were done in Hämeenlinna, Finland. Therefore the matching circuit of the first prototype was designed to cover the frequency band 498-518 MHz, which was the frequency band in the measurements. From the test results the MIMO performance of the antenna can be evaluated. The single resonant matching circuit was designed so that the antenna is almost critically coupled at 508 MHz and the -6 dB matching criterion would be fulfilled. The matching circuit was designed with the circuit simulator Aplac using optimization and tuning tools. Finally the whole antenna structure was simulated with IE3D. The matching circuit topology is shown in Figure 5.8 and the matching component values are L_1 = 43 nH and L_2 = 10 nH.

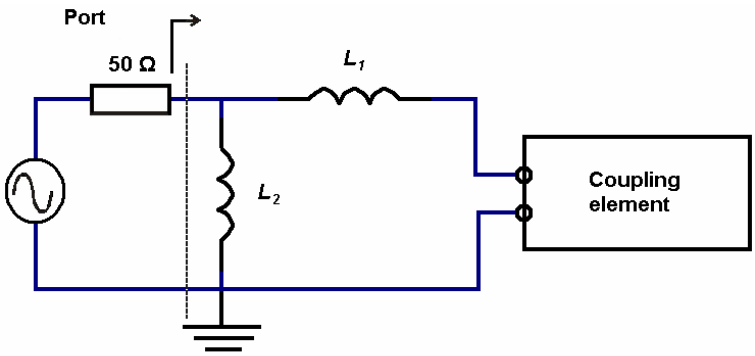

Figure 5.8: The matching circuit topology. The component values are L_1 = 43 nH and L_2 = 10 nH.

5.3.2 DUAL-RESONANT MATCHING WITH IDEAL REACTIVE COMPONENTS

Matching the full DVB-H band with a single matching circuit seems to be impossible, if the mechanical restrictions (see Figure 5.1) of the antenna are taken into account. That is why the broadband matching is implemented with two dual-resonance matching circuits per one coupling element (one for lower part of the band 470 – 550 MHz and another for the higher part 550 – 800 MHz). The structure of the matching circuit and the reference level of the S-parameters are presented in Figure 5.9. The matching circuit consists of a series and a parallel inductances and a parallel capacitance. The component values of the matching circuit are L_1 = 56 nH, L_2 = 6.8 nH and C_1 = 15 pF for the lower band and L_1 = 31.5 nH, L_2 = 5 nH and C_1 = 11.2 pF for the higher band (see Figure 5.9). The design process of the matching circuits was done with Aplac and finally the whole antenna structure was simulated with IE3D. The matching circuits had equal component values in both ports because of the symmetrical antenna structure.

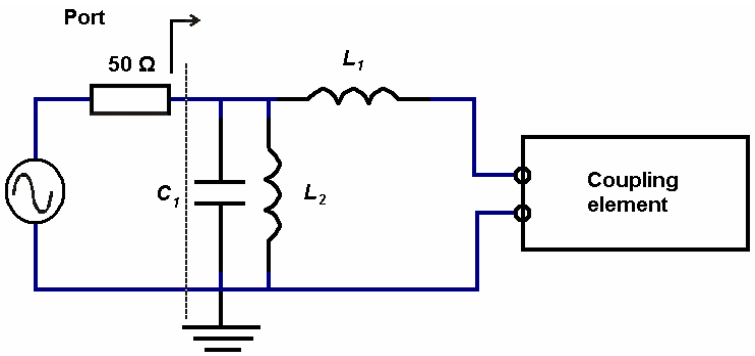

Figure 5.9: *The matching circuit topology for the dual-resonant matching.*

The desired matching circuit is chosen with RF switches [36]. In this work the switches were excluded from the prototype in order to keep measurements and the structure of the antenna prototype simple enough. The operation of the switches is difficult to predict with simulations [37] but the losses caused by the switches can be estimated and their effect to the realized gain of the antenna. The schematic structure of the antenna with the switches is presented in Figure 5.10. The final dual-element DVB-H antenna would include 4 switches and 4 matching circuits.

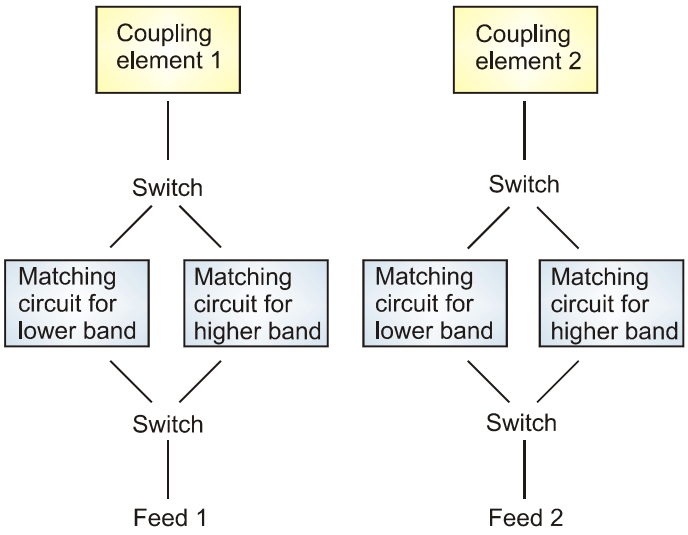

Figure 5.10: *A dual-element antenna structure with switches and matching circuits.*

Using switchable matching circuits with electrically small antennas has been studied in [38]. In that work a prototype antenna for GSM900 and GSM1800 frequency bands using two discrete lumped element matching circuits and single pole, double throw (SPDT) switches was built, measured and evaluated.

Another option to achieve a broad impedance bandwidth would be to use tunable matching components, e.g. using an electrically adjustable capacitor (varactor diode). The capacitance C_j of the varactor is defined as [11]

$$C_j = C_{j0}\left(1-\frac{V}{\phi_{bi}}\right)^{-\gamma}, \tag{5.1}$$

where C_{j0} is the capacitance without the bias voltage V, γ is the doping profile coefficient and ϕ_{bi} is the contact potential pending on the used semiconductor. With an adjustable capacitor the resonant frequency of the matching circuit can be tuned. The bias voltage can not be very high in a mobile terminal which limits the tuning range of the varactor diode. Varactors are lossy

components and their nonlinearity can cause distortion. Another drawback of the tunable matching components is that they don't operate properly if simultaneous operation of DVB-H and GSM900 is desired. The GSM antenna and the varactor diode are electrically coupled via the ground plane of the mobile terminal and the DVB-H antenna. When the GSM900 Tx transmits, currents are induced to the ground plane of the mobile terminal and these currents modulate the bias voltage of the varactor. If the bias voltage fluctuates along the modulation of the GSM signal the capacitance and the resonant frequency of the DVB-H matching circuit fluctuates also. This prevents the reception of the DVB-H signal.

5.3.3 DUAL-RESONANT MATCHING WITH REAL LUMPED COMPONENTS

The dual-resonant matching circuit with real lumped components was designed for the prototype to verify the simulation results in practice. The structure of the matching circuits is presented in Figure 5.9. The matching circuit component values are L_1 = 56 nH, L_2 = 5.6 nH and C_1 = 15 pF for the lower band (470 – 580 MHz) and L_1 = 27 nH, L_2 = 3.9 nH and C_1 = 10 pF for the higher band (580 – 800 MHz). The inductances are from Murata's LQW18A series and the capacitors are from Murata's GQM18 series. The component values are different than the ideal matching component values because real components have additional losses and reactance. The matching circuits were designed with IE3D using scattering parameters of the real lumped components. At first the whole antenna structure with matching circuits was simulated with the same real component values as in the ideal component case. If the exact component value was missing, the nearest one was picked. After this, the resonances were tuned to the desired frequencies by changing one component value at a time and checking the effect with simulations. The Smith chart presentation of the antenna impedance, absolute value of the reflection coefficient and isolation between the ports were used to design the matching circuit. Finally, the realized gain and radiation patterns of the antenna were simulated with the best matching circuit. However, the matching is not optimal dual-resonant matching because the available component values are at certain intervals and the closest possible value was chosen.

6 SIMULATION AND MEASUREMENT RESULTS

In this chapter the simulation and measurement results are reported. All the following results have been obtained with the same antenna structure (see Figure 5.4) and only the matching circuits have been changed for different frequency bands. In Section 6.1 the reflection coefficient for single-resonant matching (498-518 MHz) used in the channel measurements is presented. Simulation and measurement results are compared and the measurement setup is described. In order to evaluate the operation of the prototype antenna at the DVB-H band dual-resonant matching circuits were designed in Sections 5.3.2 and 5.3.3. In Sections 6.2 and 6.3 the reflection coefficients of the dual-resonant matched antenna design are presented. First the dual-resonant matching circuits were designed using ideal component values and finally circuits with real lumped components were implemented and tested. In Section 6.4 simulated radiation patterns, calculated envelope correlation coefficients, and simulated and measured realized gains for dual-resonant matched antenna design are presented.

6.1 Reflection coefficient for single-resonant matching

The single-resonant matching circuit was designed for the radio channel measurements (see Section 5.3.1). The reflection coefficient measurements were performed at the Radio Laboratory of TKK in the so-called impedance measurement box. The size of the box is about 1.1 x 1.1 x 1.1 m^3 and the walls of the box are covered with electromagnetic wave absorbers. The impedance box was used to prevent reflections from surroundings that would cause error to the antenna impedance measurement. The antenna was placed inside a holder (see Figure 6.1) to achieve stabile measurement conditions during the field measurements. The material of the holder was Styrofoam which has electrical properties close to air. Also the effect of the holder was examined by measuring the reflection coefficients with and without the holder. The holder didn't affect the measurement results significantly.

A VNA was used to measure the S-parameters of the prototype. The absolute values of the S-parameters for the prototype are shown in Figure 6.2. Parameters $|S_{11}|$ and $|S_{22}|$ are the reflection coefficients in port 1 and port 2, respectively, and $|S_{21}|$ represents the isolation between the ports. The absolute value marks have been excluded from the latter parts of this thesis.

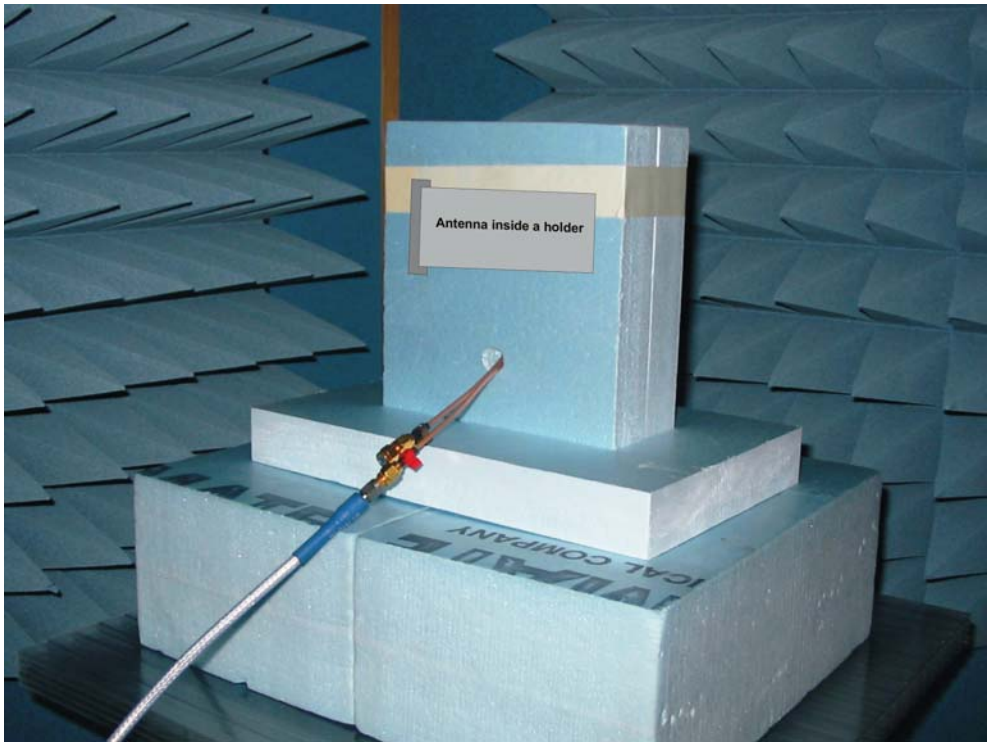

Figure 6.1: *The S-parameter measurement setup. The prototype was placed inside the holder and the measurements were performed in the impedance box.*

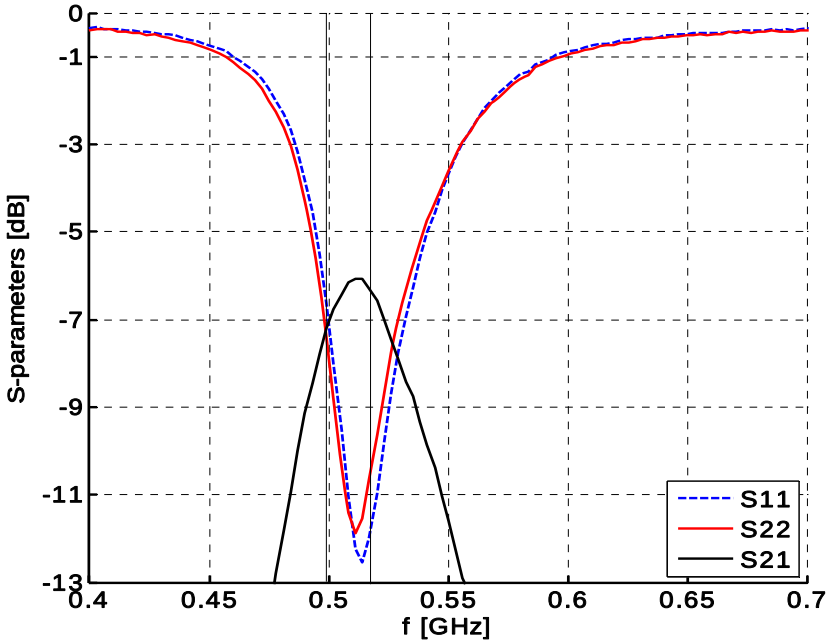

Figure 6.2: *Measured scattering parameters of the prototype. The desired frequency band was 498 – 518 MHz.*

In Figure 6.3 the simulated and the measured reflection coefficients are compared and it can be seen that the measured and the simulated results differ a little. It was noticed that by increasing the inductance with 3 nH in the simulations the simulation results agreed better with measurement results. The prototype seems to have about 3 – 4 nH higher series inductance than the simulation model. This can be caused by the connection between the feed cable and the microstrip line (see Figure 6.4) which was not included in the simulation model of the antenna.

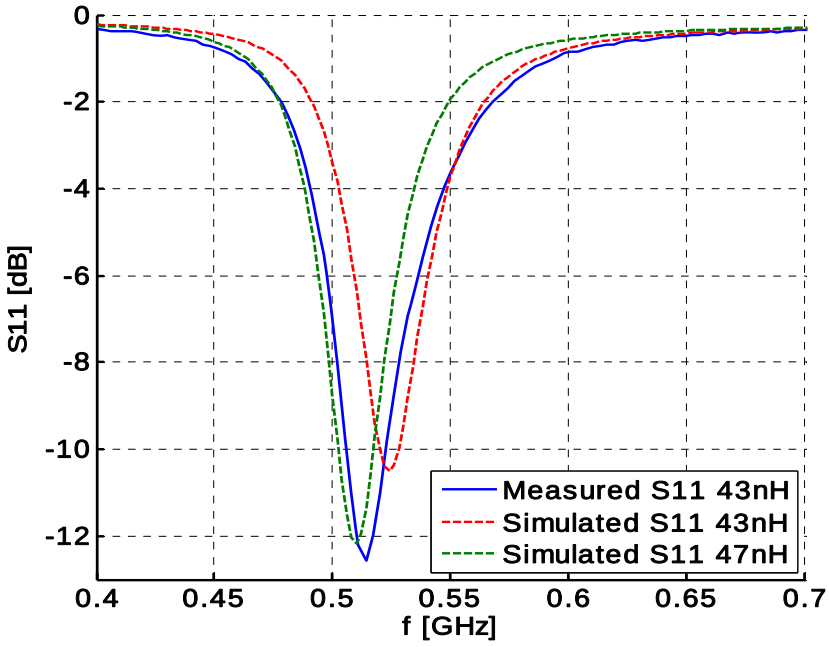

Figure 6.3: *A comparison between the measured and the simulated reflection coefficients of the prototype with two different series inductances.*

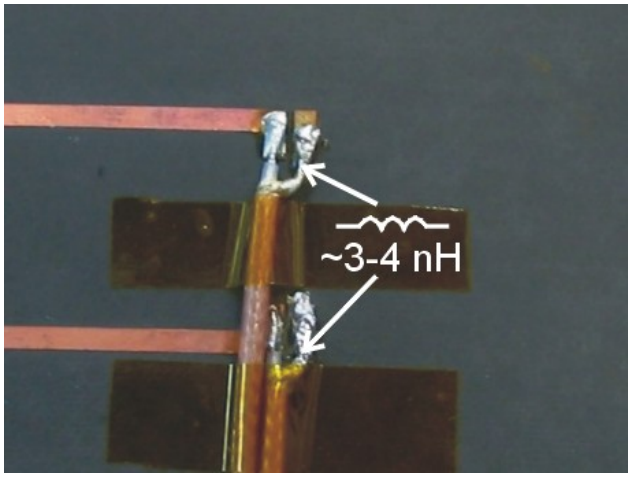

Figure 6.4: *A "pigtail" connection between the feed cable and the microstrip line.*

6.2 Reflection coefficient for dual-resonant matching with ideal component values

In Figure 6.5 the simulated reflection coefficients for dual-resonant matching with ideal reactive components are presented. The design process of the matching circuit is presented in Section 5.3.2. The blue curve presents matching for the lower band (470 – 550 MHz) and the red curve for the higher band (550 – 800 MHz). The reflection coefficient is less than -1.2 dB at the lower band and less than -1.5 dB at the higher band. S_{11} is equal to S_{22} because the structure of the antenna is symmetric and the matching circuits are similar in both ports. The ports of the antenna structure have been defined in Figures 5.4 and 5.9. As can be seen from Figure 6.5, matching the lower band is much more challenging than matching the higher band. According to Equation (2.17) $Q_{rad,min}$ increases if the frequency is decreased and this is why the achievable bandwidth decreases at low frequencies.

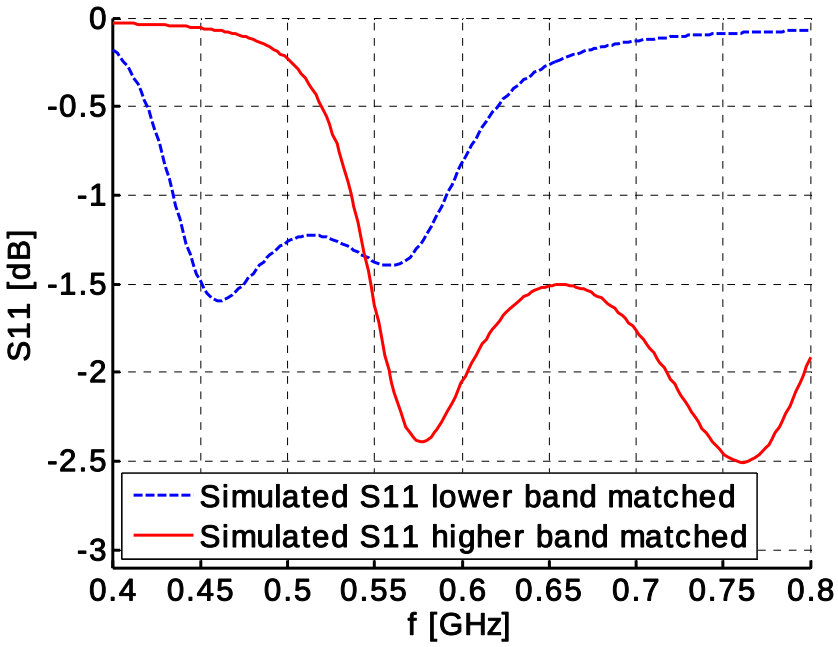

Figure 6.5: *Simulated reflection coefficients with the dual-resonant matching circuits. These simulations were done using ideal component values.*

These results with ideal components are presented because the radiation patterns of this design were used in MEBAT simulations (see Chapter 7). The matching circuits with real lumped components were not designed yet when the MEBAT simulations were done.

6.3 Reflection coefficient for dual-resonant matching with real components

The reflection coefficient measurements of the prototype with the dual-resonant matching circuits and real lumped components were done with a VNA in the impedance measurement box, described in Section 6.1. In the simulations the matching circuit components were modelled using the scattering parameters of the real components. The structure and component values of the matching circuit are presented in Section 5.3.3. The measured and the simulated reflection coefficients with real matching components are presented in Figures 6.6 and 6.8 for the lower band and for the higher band, respectively. The isolations of the ports are presented in Figure 6.7 for the lower band and in Figure 6.9 for the higher band. The simulated matching is about 0.5 dB better than with the ideal components. This is mainly due to losses in real components. On the other hand losses deteriorate the realized gain. Also RF switches, that would be included in the final antenna, add losses to the system.

The simulated and the measured reflection coefficients are less than -2 dB and -2.5 dB, respectively, at the whole lower band. The differences between the measured reflections coefficients S_{11} and S_{22} are due to differences in the mechanical structure of the prototype and variation in the lumped component values. The simulated isolation of the ports is higher than 7 dB and the measured isolation is higher than 8 dB at the lower band. The isolation depends on the matching and the lowest isolation is attained when the antenna is well matched. This is why the isolation can be increased by redesigning the matching circuit and lowering the matching. The isolation also depends on the mechanical structure of the antenna.

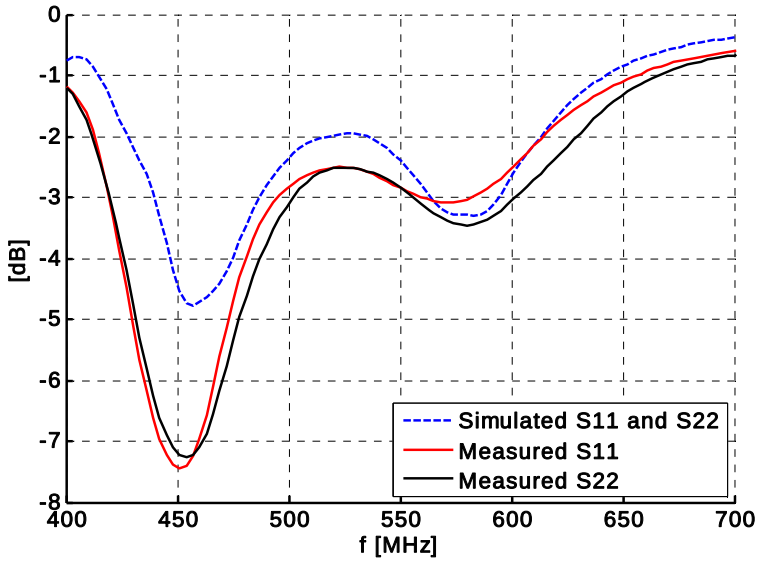

Figure 6.6: *The simulated and the measured reflection coefficients for the both ports. The dual-resonant matching circuit for the lower band (470 – 580 MHz) was used.*

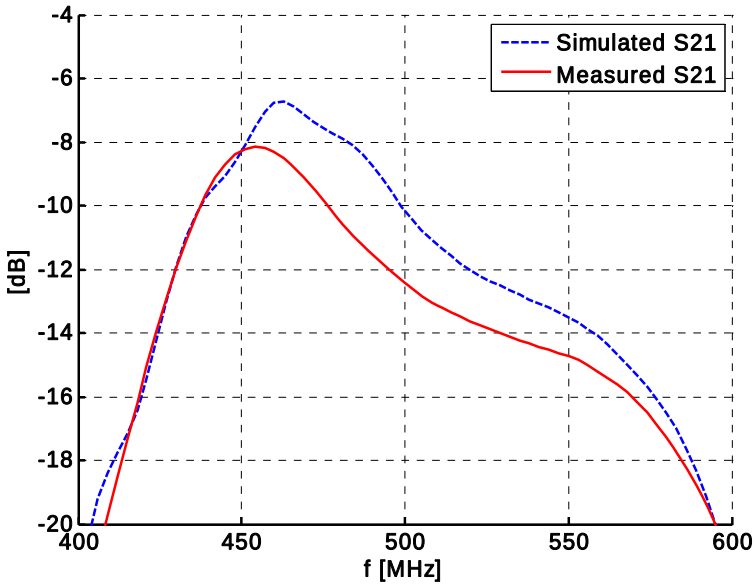

Figure 6.7: *The simulated and the measured isolation of ports 1 and 2. The dual-resonant matching circuit for the lower band (470 – 580 MHz) was used.*

The maximum reflection coefficient for the higher band is -2 dB. The measured and simulated results agree quite well. The minimum isolation of the ports is 9 dB for the higher band which is a few dB better than the isolation for the lower band. Again, the lowest isolation is attained when the reflection coefficient is at the minimum.

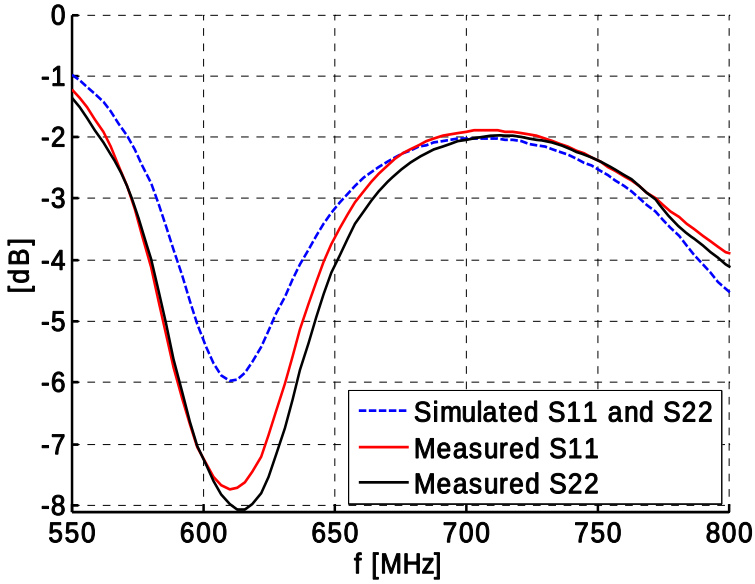

Figure 6.8: *The simulated and the measured reflection coefficients for the both ports. The dual-resonant matching circuit for the higher band (580 – 800 MHz) was used.*

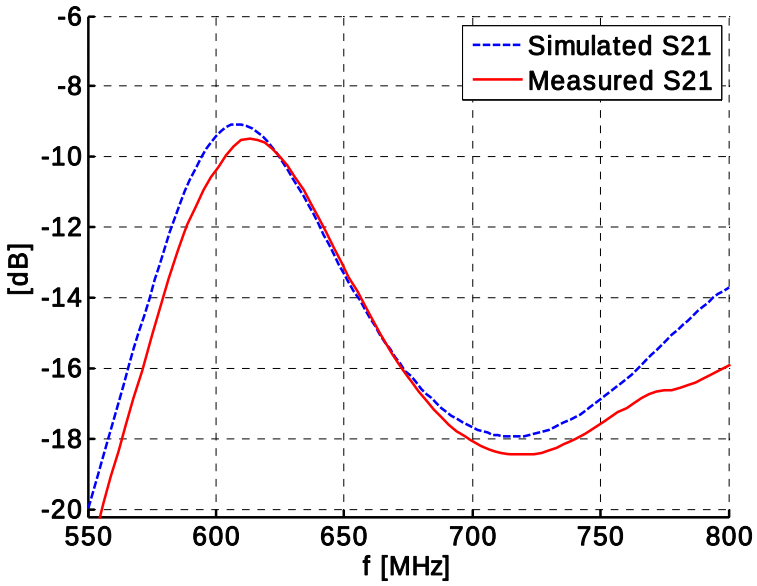

Figure 6.9: *The simulated and the measured isolation of ports 1 and 2. The dual-resonant matching circuit for the higher band (580 – 800 MHz) was used.*

6.4 Radiation patterns, envelope correlation and realized gain

Radiation patterns and realized gain of the antenna were simulated with IE3D. The dual-resonant matching circuits (see Figure 5.9) with ideal component values were used in the simulations. The simulated 3-D radiation pattern and the polarization ellipses of the antenna at 700 MHz are presented in Figure 6.10 in the horizontal orientation and in Figure 6.11 in the vertical orientation. These radiation patterns were used in MEBAT simulations described in Chapter 7. The patterns were simulated with IE3D and they have been drawn with a Matlab code originally developed by Jussi Rahola.

The patterns are quite similar to the radiation pattern of a dipole antenna. From Figure 6.10 it can be seen that the directional nulls are turned about 40° when the feed is switched from port 1 to port 2. In the horizontal orientation (Figure 6.10) the polarization ellipses are quite similar when comparing different ports and in the horizontal plane (θ = 90°) the antenna is almost linearly polarized. In the vertical orientation (Figure 6.11) the polarization ellipses are more tilted when the feed is in different ports and in the horizontal level the polarization of the antenna is a combination of the horizontal and the vertical polarization. This is why higher polarization diversity could be achieved with the vertical orientation than with the horizontal orientation.

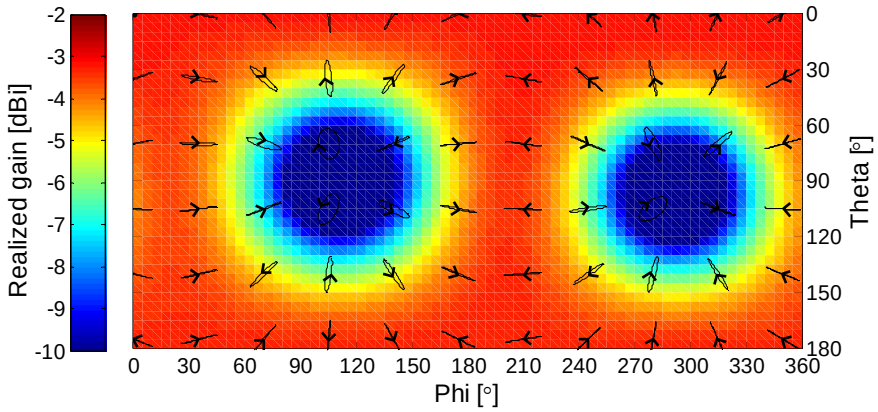

(a)

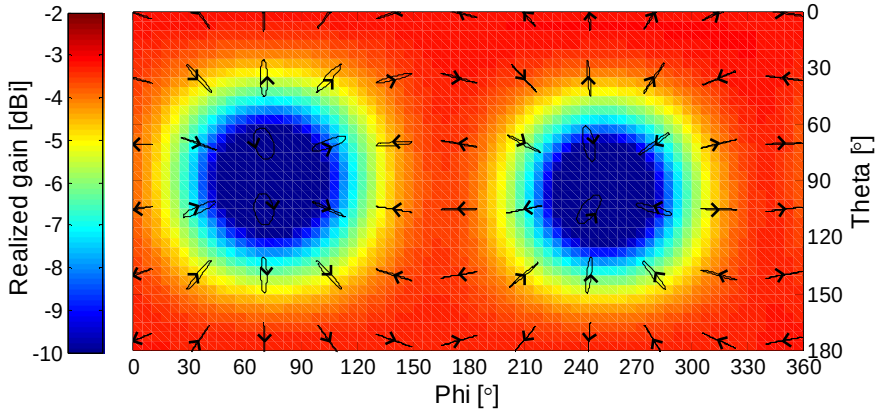

(b)

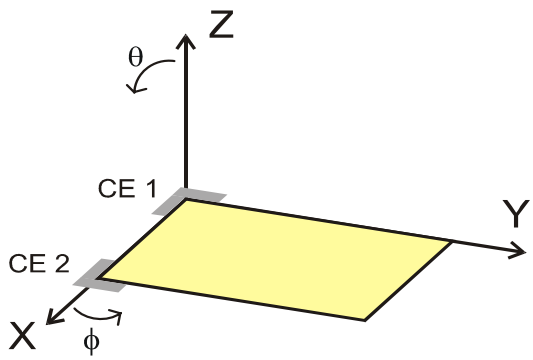

(c)

Figure 6.10: *The radiation patterns and polarization ellipses at 700 MHz with dual-resonant matching circuit. The feed of the antenna is (a) in port 1 and (b) in port 2. (c) The orientation of the antenna.*

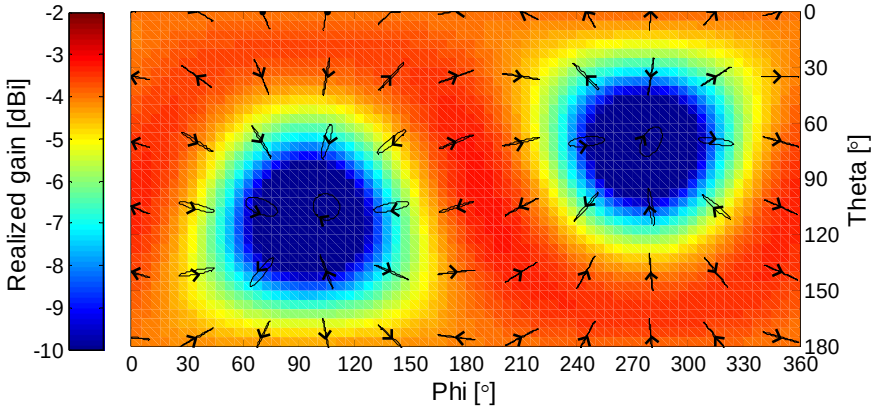

(a)

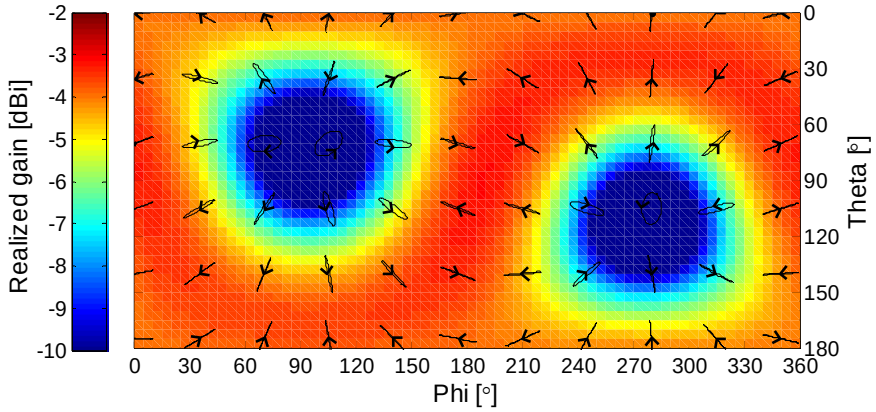

(b)

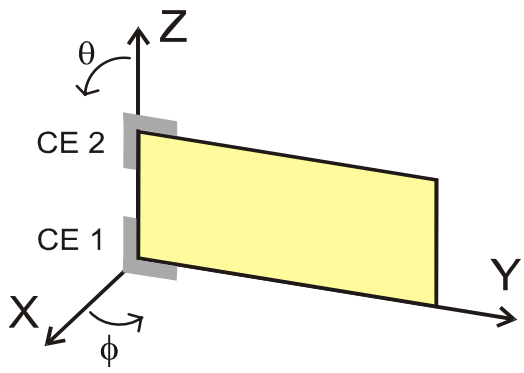

(c)

Figure 6.11: *The radiation patterns and polarization ellipses at 700 MHz with dual-resonant matching circuit. The feed of the antenna is (a) in port 1 and (b) in port 2. (c) The orientation of the antenna.*

The calculated envelope correlation coefficients (Equation (3.1)) of the prototype with dual-resonant matching circuits and ideal matching components (presented in Section 5.3.2) are presented in Figure 6.12. The envelope correlation is under 0.6 at the desired frequency bands. As mentioned in Section 3.1.1, the envelope correlation value 0.7 has often been used as an upper limit of the correlation for diversity applications.

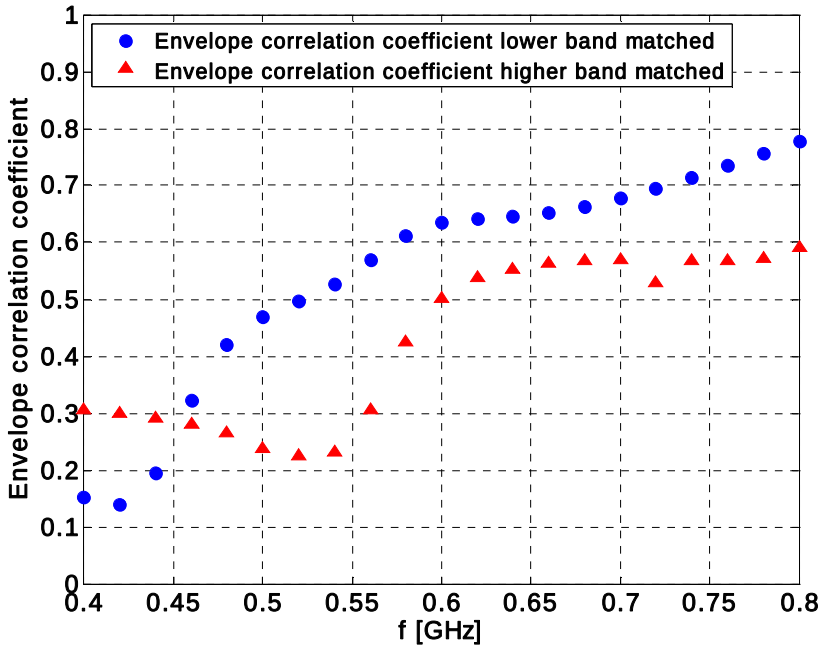

Figure 6.12: *Simulated envelope correlation coefficient. The dual-resonant matching circuits with ideal matching components were used. The lower band is 470 – 550 MHz and the higher band is 550 – 800 MHz.*

The simulated the maximum realized gains of the prototype antenna with dual-resonant matching circuits and ideal matching components are presented in Figure 6.13. The used frequency band was the whole DVB-H band which was divided into lower (470 – 550 MHz) and higher (550 – 800 MHz) sub-bands. It can be seen that the realized gain specification is fulfilled with a 2.5 dB margin. The real matching components and the switches cause losses to the system and deteriorate the realized gain. On the other hand, losses improve impedance matching and the realized gain can be increased by optimizing the matching component values better or increasing the size of the coupling elements if the margin is not sufficient. However, the antenna structure is so small compared to the wavelength at low frequencies (470 – 500 MHz) that improving the impedance matching may not affect the realized gain much because the radiation efficiency of the antenna is so low. This can be seen by comparing Figures 6.13

and 6.5. The reactive near fields are dominant and they store much more energy than the radiated fields.

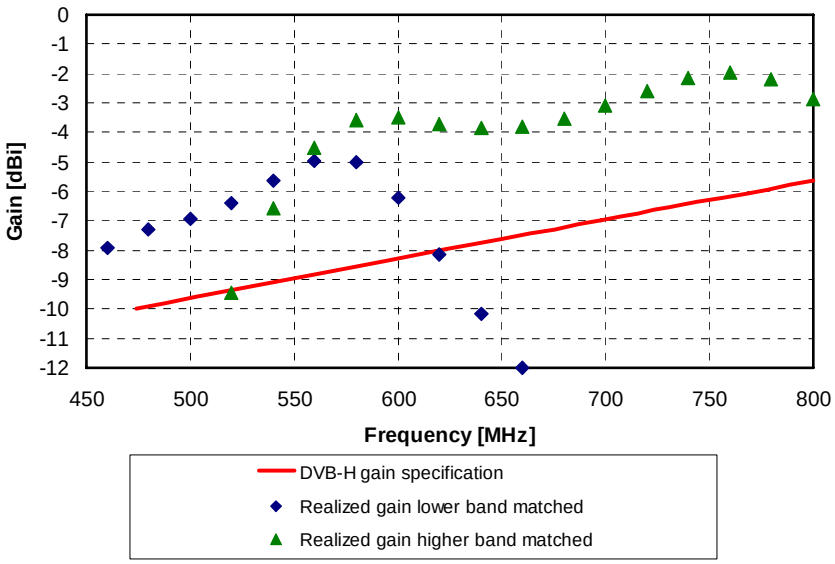

Figure 6.13: *Simulated maximum realized gains with the dual-resonant matching circuits and ideal component values.*

The realized gain measurements of the dual-resonant matched antenna prototype were carried out at the Radio Laboratory in a small anechoic chamber. The schematic representation of the measurement setup is presented in Figure 6.14. The measured antenna was set as a transmitting antenna and a dual-polarized Vivaldi antenna (ETS-Lindgren's series 3164-03) was operating as a receiver antenna. Horizontal and vertical polarizations can be measured separately using the Vivaldi antenna. When the horizontal polarization was measured the cable from the vertical polarized antenna was terminated with a 50 Ω load and vice versa. A VNA was set to measure the power flow from port 1 to port 2. The full 3-D radiation pattern was then measured by rotating the antenna under test (AUT) in the azimuth plane ($\varphi = 0° \rightarrow 360°$) and in the elevation plane ($\theta = 0° \rightarrow 180°$). The realized gain of the dual-element prototype antenna was measured using comparison method [39].

$$G_{AUT} = \frac{P_{AUT}}{P_{ref}} \cdot G_{ref}, \tag{6.1}$$

where P_{AUT} and P_{ref} are the powers transferred by the antenna under test and the reference antenna, respectively, and G_{ref} is the realized gain of the reference antenna. The received powers were obtained by integrating the measured radiation pattern over a spherical surface and summing up the powers of two polarizations. The reference antennas were half-wave dipoles

and their gain is G_{ref} = 2 dBi. For the dipole antennas the realized gain G_r equals to gain G because they are very well matched at the operating frequency.

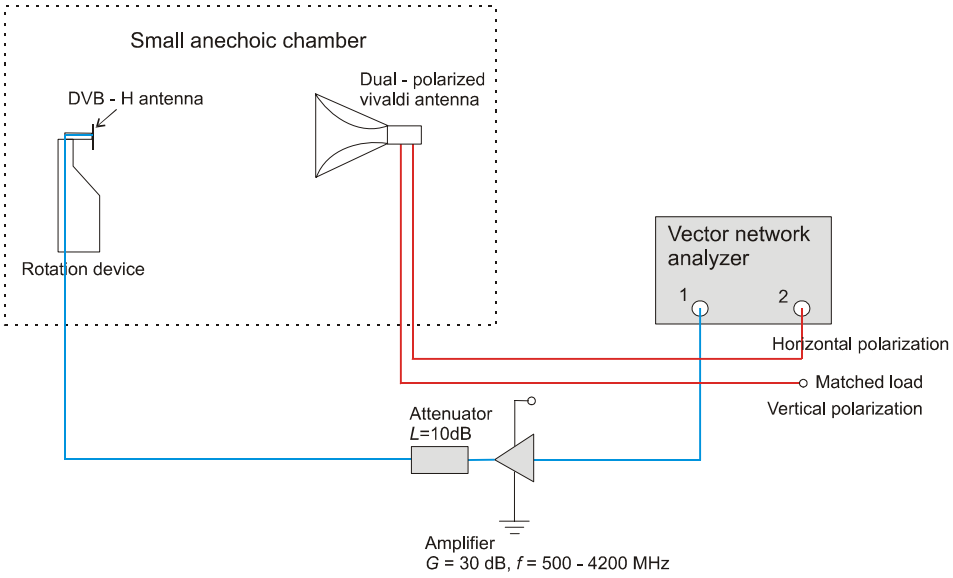

Figure 6.14: *The radiation pattern measurement system.*

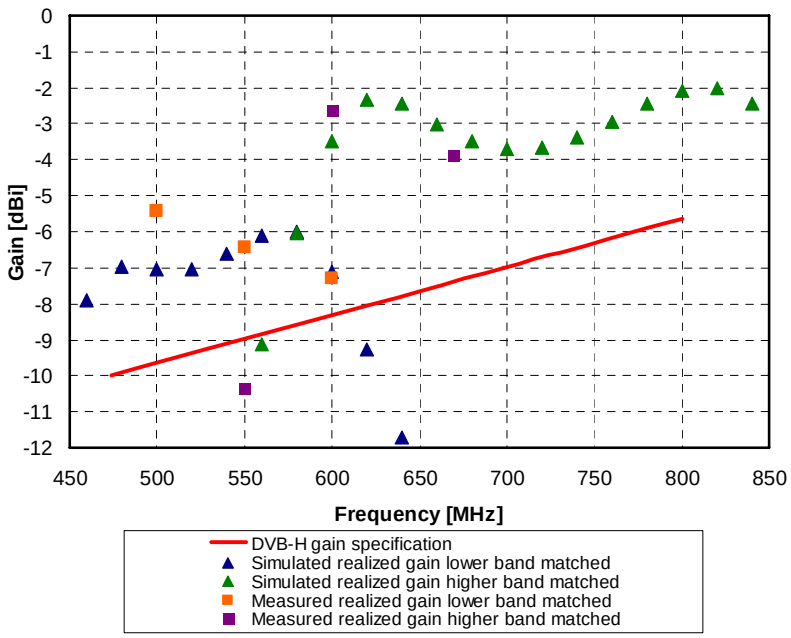

Figure 6.15: *The simulated and measured maximum realized gains with the dual-resonant matching circuits and real lumped matching components.*

The simulated and the measured maximum realized gains are presented in Figure 6.15. In the simulations the matching circuit components were modelled with scattering parameters of the real lumped components. The lower band matching covers the sub-band 470 – 580 MHz and the higher band matching covers the sub-band 580 – 800 MHz. The DVB-H specification is fulfilled with about 2.5 dB margin. The reference dipole antennas have been designed at 500, 550 and 670 MHz. The gain result at 600MHz was calculated so that the power of the reference dipole antenna was interpolated from the powers at 550 MHz and 670 MHz. Measured results correspond well to the simulated results. At 500 MHz the measured realized gain is 1.5 dB higher than the simulated realized gain. This can be due to the better matching of the measured prototype compared to the simulation model or measurement uncertainties. The performance of the anechoic chamber has not been verified at such a low frequency and this can also have an effect to the measurement results. At low frequencies the absorption materials are not working properly and reflections may occur. The reflected power can be absorbed by the receiving antenna and received power increases. Also the gain of the reference antenna can differ a little from 2.5 dB and this causes error to the measurement.

7 MIMO PERFORMANCE ANALYSIS WITH MEBAT

In this Chapter the MIMO performance of the antenna is evaluated in different propagation environments using a tool called MEBAT. First, a short introduction to MEBAT is given in Section 7.1. Mutual information, spatial multiplexing efficiency and transmitted signal power gained with the prototype are compared with these of a single-element antenna which has the same total volume as the prototype. This reference antenna is introduced and reported in Section 7.2. The used propagation environments are presented in Section 7.3. Finally, the simulation results are presented in Section 7.4.

7.1 Introduction to MEBAT

Traditionally, antennas have been evaluated according to the different radiation characteristics like gain, efficiency and radiation pattern. These characteristics can be measured in an anechoic chamber. However, in the real user environment the signal distribution is not uniform and the received signal depends on the signal propagation environment. Several copies of the same Tx signal arrive from different directions and with different delays. The received signal power depends on the orientation and the radiation pattern of the Rx antenna. The most accurate way to evaluate the antenna in a real propagation environment is a direct sounder measurement. At the same time it is also the most time consuming method [40]. The basic idea of MEBAT is presented in Figure 7.1. The signal distribution in a real environment can be estimated by performing channel sounder measurements and using a spherical antenna array at the receiver end. Then a set of plane waves (described by blue arrows in Figure 7.1) is formed from the measurement results. The plane wave estimation can by done by using e.g. a beamforming algorithm [22]. The complex 3-D radiation pattern of the Rx antenna can be simulated or measured in anechoic chamber. The effect of the user can also be included in the radiation pattern. After this, the channel matrix $\mathbf{H}(t)$ (3.2) that includes the effect of Tx and Rx antennas can be calculated by combining the estimated signal distribution and the complex 3-D radiation pattern of the prototype antenna [22]. The power normalization of the channel matrix is done with an ideal dual-polarized isotropic antenna array. Because the normalization antenna is ideal the absolute values of the simulation results are low.

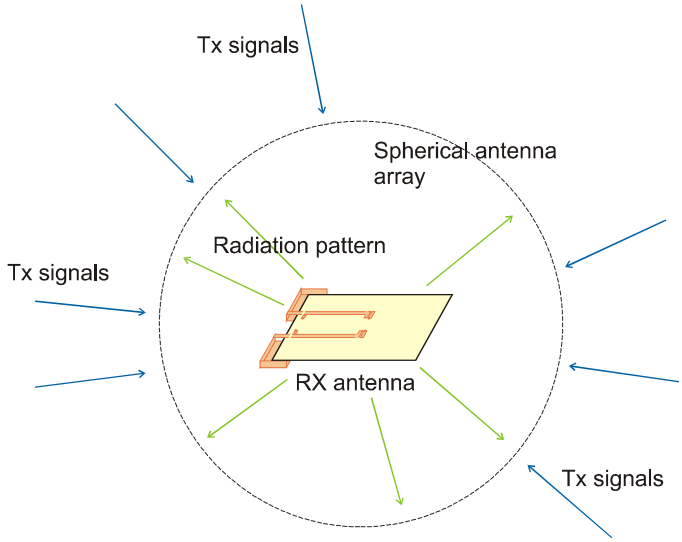

Figure 7.1: *The basic idea of MEBAT.*

MEBAT simplifies the antenna evaluation process as compared with direct measurements, as the same measured channel data can be utilized to evaluate different antenna prototypes. In practice, MEBAT is a Matlab program combining the basic evaluation method and a propagation channel data library. The evaluation method that is used in MEBAT is called the experimental plane-wave based method (EPWBM) [22]. The block diagram of the basic difference between the direct measurement and the EPWBM is presented in Figure 7.2. The EPWBM requires the directional channel measurements and the channel estimation but once they have been made the same channel data can be exploited in various simulations with different Rx radiation patterns. The radiation pattern of the Rx antenna can be rotated in the azimuth and elevation planes. Usually the antenna is rotated in the azimuth plane $\phi = 0° - 360°$ and the results with different angles are combined.

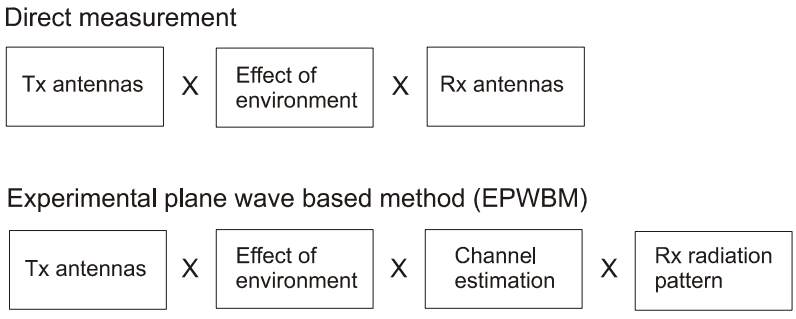

Figure 7.2: *Basic difference between the direct measurement and EPWBM [22].*

In this work the channel measurements for MEBAT simulations were done with the channel sounder developed for 2 GHz frequency range [41]. The 2 GHz data was used because

propagation data below that frequency was not available. According to a short literary research, MIMO channel measurements have not been reported at DVB-H frequency range. This is of course a problem because the differences between the signal propagation in a real environment at 2 GHz and e.g. 700 MHz are not known. However, if the simulations are done with a proper reference antenna one can at least compare the results and have a conception of the performance differences between different antennas. In this work the dual-element prototype has been compared to a single-element reference antenna in order to gain knowledge whether it is useful to have several antenna elements in a DVB-H receiver.

The antenna arrays used in the channel measurements are presented in Figure 7.3. The spherical receiver antenna array used in the mobile end consists of 32 elements mounted on a spherical surface as in Figure 7.3 (a). Each element has two feeding probes corresponding to orthogonal linear polarizations. The array elements are half-wavelength rectangular stacked microstrip patches with air substrate [41]. The transmitter antenna arrays used as base station antennas consist of 16 antenna elements similar to those used in the Rx array. In the linear antenna array (see Figure 7.3 (b)) the array elements are mounted on a plane in a straight line. The element spacing is 0.7 λ. In the zigzag antenna array, presented in Figure 7.3 (c), the element spacing is 0.7 λ.

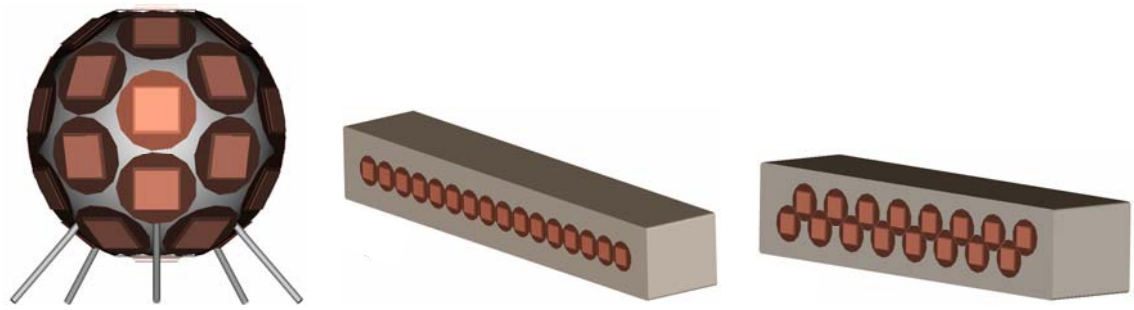

(a) (b) (c)

Figure 7.3: *(a) Spherical Rx antenna array, (b) Linear Tx antenna array, and (c) zigzag Tx antenna array.*

The evaluated prototype radiation patterns can be seen from Figures 6.10 and 6.11. The 3-D radiation patterns are simulated at 700 MHz with dual-resonant matching circuits and ideal matching components (see Section 5.3.2). In the MEBAT simulations two different elevation alignments were analyzed. In the simulation results Proto1 000 corresponds to the antenna position in Figure 6.10 (c) and Proto1 090 corresponds the antenna position in Figure 6.11 (c). In MEBAT simulations the antenna was rotated in the azimuth plane. Each following simulation

result includes six different azimuth alignments of the antenna. The rotation has been done at 60° intervals, so that the whole azimuth plane has been analyzed.

7.2 Reference antenna

In the MEBAT simulations a single-element DVB-H antenna was used as a reference antenna. The single-element antenna was chosen as a reference in order to gain knowledge on whether there are any advantages if the dual-element antenna is used instead of the traditional single-element antenna system (single-input single-output (SISO)) at DVB-H frequency band. The structure of the reference antenna is presented in [33]. The dimensions of the antenna in [33] were modified so that it has the same total volume (2.05 cm^3) as the dual-element prototype. Also the dimensions of the ground plane were changed to correspond the ground plane of the dual-element prototype. The structure and the dimensions of the reference antenna are presented in Figure 7.4.

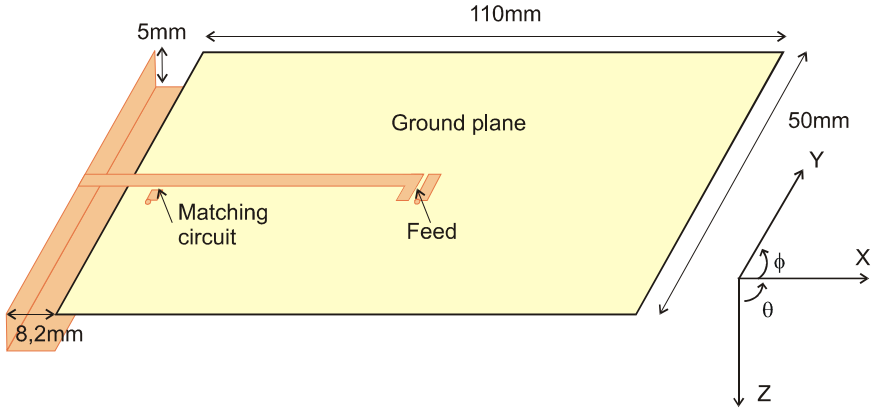

Figure 7.4: *The structure and the dimensions of the single-element reference antenna.*

One dual-resonant matching circuit (see Figure 5.9) was used to match the antenna at 550 – 800 MHz. This matching circuit was first designed using Aplac optimization tools and the final tuning was done using IE3D. The whole antenna structure with the matching components was simulated with IE3D and by means of Smith chart presentation of the reflection coefficients the suitable matching components were chosen. The component values of the matching circuit are L_1 = 23.5 nH, L_2 = 3.1 nH and C_1 = 16.9 pF. Ideal reactive component values were used in the simulations. In order to match the whole DVB-H band, two dual-resonant matching circuits and two RF switches would be needed as in the dual-element prototype case (see Figure 5.10). The reflection coefficient of the reference antenna has been presented in Figure 7.5. The reflection coefficient of the dual-element prototype is shown in the same picture for comparison.

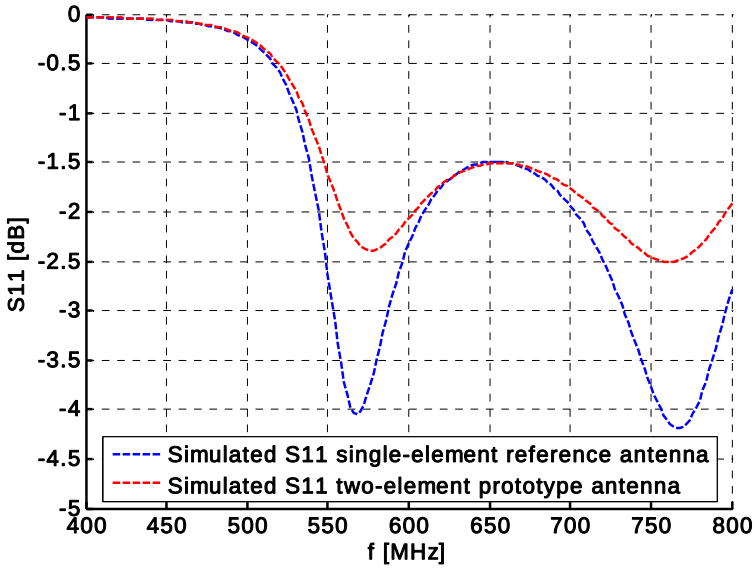

Figure 7.5: *The simulated reflection coefficient of the single-element reference antenna and the dual-element prototype (from Section 6.2). The desired frequency band is 550 – 800 MHz.*

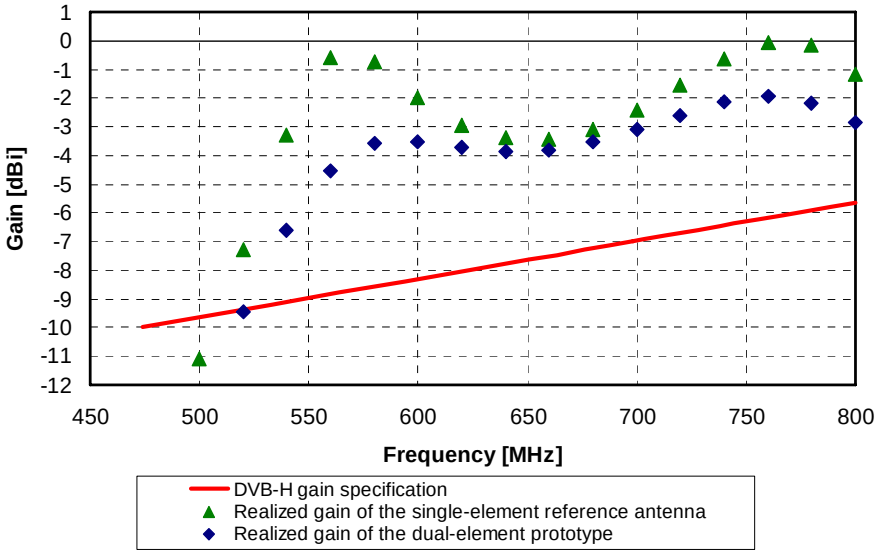

Figure 7.6: *The simulated maximum realized gain of the single-element reference antenna and the dual-element prototype. The higher band was matched using ideal matching components. The red line presents the DVB-H specification. The evaluation frequency was 700 MHz in the MEBAT simulations.*

The simulated maximum realized gains of the reference antenna and the dual-element prototype are presented in Figure 7.6. From the figure it can be seen that the realized gain of the single-element antenna is higher than the realized gain of the dual-element prototype. This is due to the larger size of the coupling element. The coupling is also stronger when the distance between the

coupling element and the ground plane is increased. For the reference antenna the distance is 8.2 mm (see Figure 7.4) and for the prototype it is 7 mm at the short side and 5 mm at the long side of the ground plane (see Figure 5.4). That is why the reference antenna has better matching and higher realized gain than the dual-element prototype. It can be said that the reference antenna is quite an ideal internal single-element DVB-H antenna. The radiation pattern of the reference antenna is similar to the radiation pattern of a thick dipole. Later in the MEBAT results the reference antenna has been referred to as SISO.

7.3 Channel data measurement environments

Indoor picocell MIMO measurements with the spherical Rx and the linear Tx antenna arrays have been carried out in 2001 at TKK at the Department of Computer Science and Engineering. The receiver was moved around the ground floor on a trolley. The measurement routes A and B are presented in Figure 7.7. The transmitter was situated in the centre part of the building on the top of a wooden "tower". The height the transmitter antenna was 3.8 m from the ground floor. [40], [42]

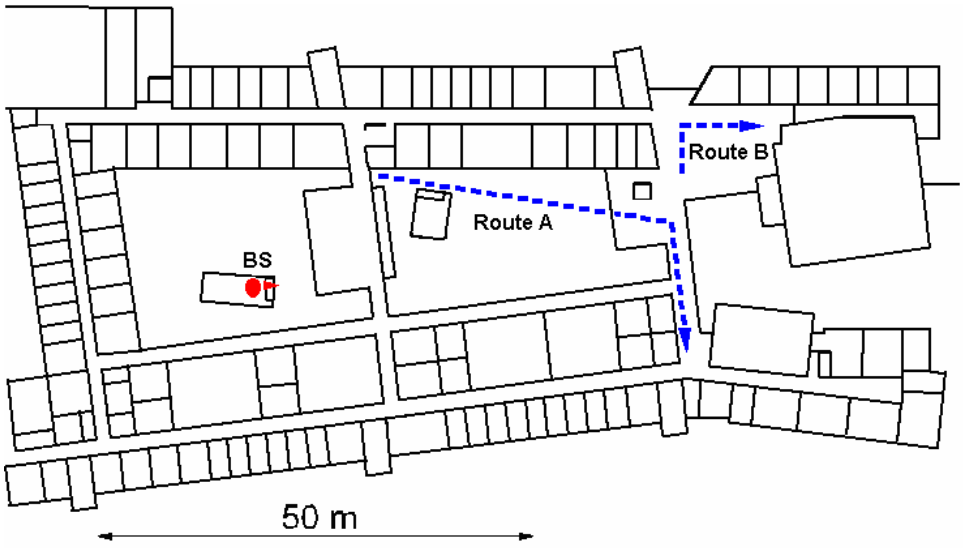

Figure 7.7: *The measurement routes in indoor picocell environment and the location of the base station antenna.*

Outdoor small macrocell measurements have been performed with the dual-polarized zigzag array in the transmitter end and the spherical array in the receiver end in Helsinki city centre. The receiver was placed on a trolley and was moved on a route presented in Figure 7.8. The base station was located on the rooftop parking lot. [42]

Outdoor microcell measurements with the spherical Rx antenna array and the zigzag Tx array have also been performed in downtown Helsinki. The receiver was placed on a trolley and was driven along a route presented in Figure 7.9. The base station was located on a crane and the height of the transmitter was 13 m from the ground level. [40], [42]

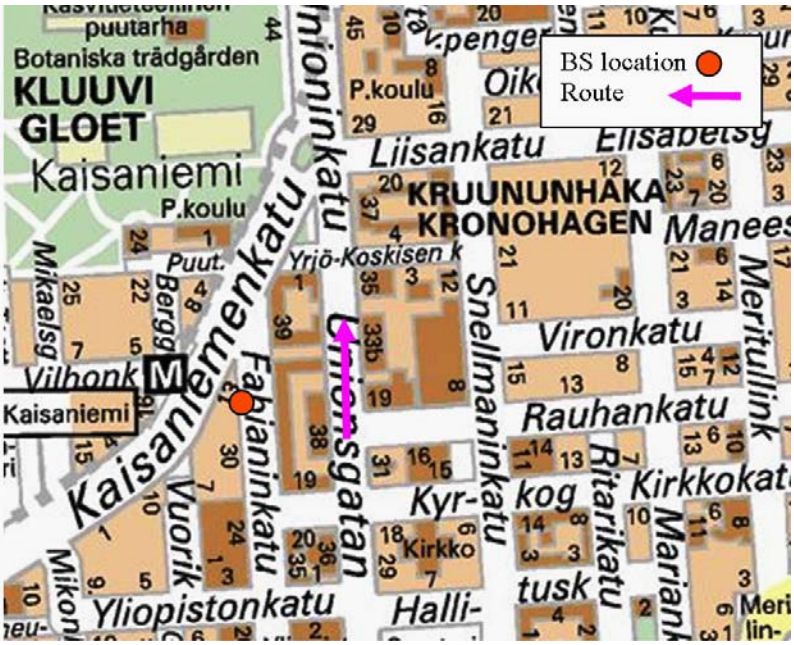

Figure 7.8: *The measurement route and the location of the base station in outdoor small macrocell environment.*

Figure 7.9: *The measurement route and the location of the base station in outdoor microcell environment.*

7.4 MEBAT results in the outdoor small macrocell environment

The small macrocell environment results have been selected under closer examination because from the three environments it is closest to the typical DVB-H propagation scenario. Typically the DVB-H transmitter is placed on a radio tower and the distance between the transmitter and the receiver is a few kilometers. In the channel measurements the distance has not been this long. On the other hand, if the distances are compared at wavelengths the difference is not so large because the wavelength at 2 GHz is about one third of the wavelength at the center frequency of the DVB-H band. Results for indoor picocell and outdoor microcell environments, described above, are presented in Appendix I (see Figures A.1 – A.4). These results have not been analyzed separately because they correspond well to the results of the small macrocell environment. The highest mutual information is achieved in the indoor environment and the results in the microcell environment and in the small macrocell environment are almost equal. In the Appendix only the mutual information results are presented because it is the most significant figure of merit, when the MIMO performance of the antenna is evaluated. The spatial multiplexing efficiency (3.5) and the transferred signal power (3.4) are included in the mutual information (3.3).

In the following figures Proto1 refers to the dual-element prototype with dual-resonant matching circuits and ideal matching components and SISO refers to the single-element reference antenna. The orientation 000 refers to the horizontal antenna orientation in Figure 6.10 (c) and 090 refers to the vertical orientation in Figure 6.11 (c). In all simulations the SNR value has been 10 dB and the evaluation frequency has been 700 MHz.

7.4.1 DUAL-POLARIZED TRANSMITTING ANTENNA

In these simulations only one element of the linear array antenna was used in the transmitter end. Both θ and ϕ polarizations from this dual-polarized Tx element were used when the dual-element prototype was analyzed and for the single-element reference antenna only the ϕ polarization was used. The mutual information results at different outage probability levels in the small macrocell environment are presented in Figure 7.10. For example, if the mutual information is 1 bits/s/Hz at the 0.4 outage probability level it means that the probability that the mutual information is below 1 bits/s/Hz is 40 %. From the Figure it can be seen that the greatest benefit from the use of the dual-element antenna is attained at high reliability levels. This is a good result because television signal is continuous and blackouts are not desired. On the other hand, DVB-H signal is send in bursts and also error correction algorithms are used to prevent

breaks in the television picture and sound although short blackouts in signal transmission would occur.

From Figure 7.10 it can be seen that the mutual information of the dual-element antenna depends on the orientation of the antenna. The reason for the difference can be examined from the 3D radiation patterns (Figures 6.10 and 6.11), as described in the following text. Most of the received signals are coming slightly above the horizontal plane [42] and that is why the $\theta = 90°$ plane is the most significant in the radiation patterns. From Figure 6.10 (horizontal orientation) it can be seen that in the horizontal plane the antenna is almost horizontally polarized. In Figure 6.11 (vertical orientation) there is a clear difference in the polarization ellipses when comparing the different ports and they are also tilted. The vertical orientation is better when the dual-polarized Tx antenna is used because the signal can be received with both θ and ϕ polarizations. Also higher diversity gain can be achieved when the polarization ellipses differ from each other. Because the radiation pattern of the single-element antenna is similar to the radiation pattern of the dipole antenna the elevation rotation has no effect on the received signal power and mutual information results.

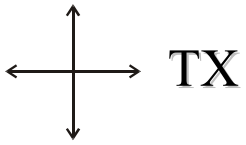

(a)

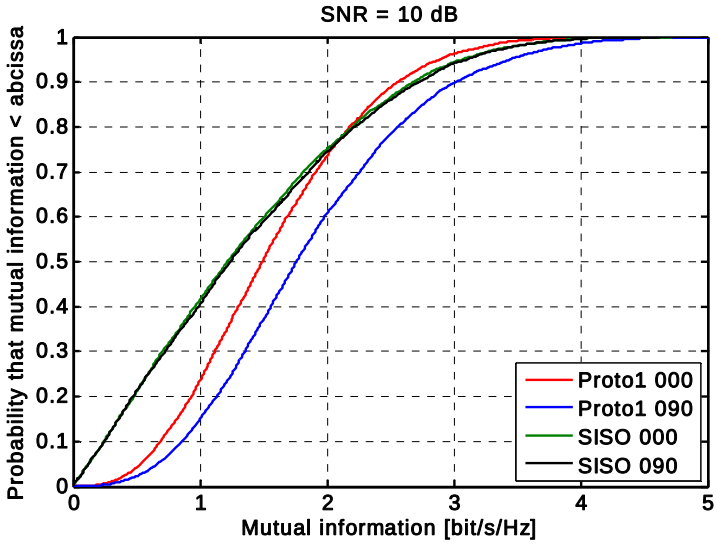

(b)

Figure 7.10: *(a) The dual-polarized Tx antenna and (b) mutual information with SNR = 10 dB.*

The mutual information results in small macrocell environment with dual-polarized Tx antenna are presented in Figure 7.10. At the 10 % outage probability level the mutual information of the dual-element antenna is about 170 % higher in the horizontal orientation and about 250 % higher in the vertical orientation compared to single-element reference antenna. At the 50 % outage probability level the mutual information is 21 % higher when using the dual-element antenna in the horizontal orientation compared to single-element reference antenna. The mutual information is 42 % higher when using the dual-element antenna in the vertical orientation. The absolute values of the mutual information results at the 10 % and 50 % outage probability levels are presented in Table 7.1.

Table 7.1: *Mutual information with the dual-polarized Tx antenna.*

Outage probability level	Mutual information [bit/s/Hz]		
	SISO	Proto1 000	Proto1 090
10 %	0.25	0.69	0.86
50 %	1.25	1.48	1.76

The spatial multiplexing efficiency for the dual-element prototype is presented in Figure 7.11. The vertical orientation has higher multiplexing efficiency at all probability levels. At the 10 % outage probability level the vertical orientation is 2 bit/s/Hz better than the horizontal orientation. At the 50 % level the difference is 1.4 bit/s/Hz.

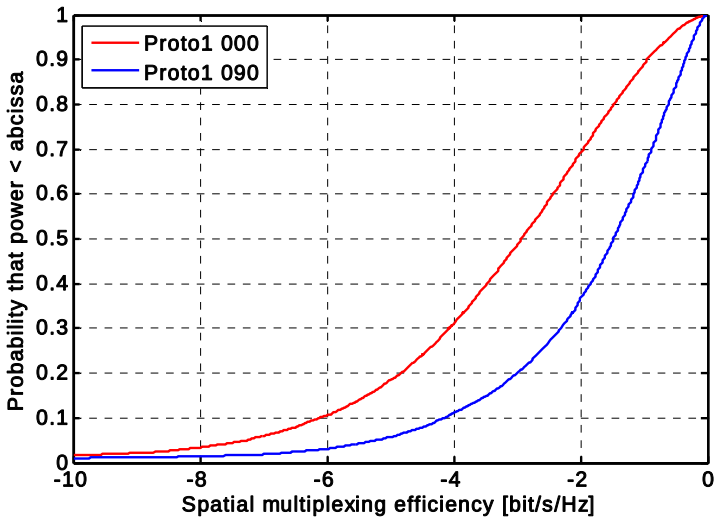

Figure 7.11: *Spatial multiplexing efficiency with the dual-polarized Tx antenna.*

The transferred signal power is presented in Figure 7.12. At the low outage probability levels the signal power transferred by the dual-element prototype is higher but at higher outage probability levels (> 0.35) the single-element reference antenna transfers more power.

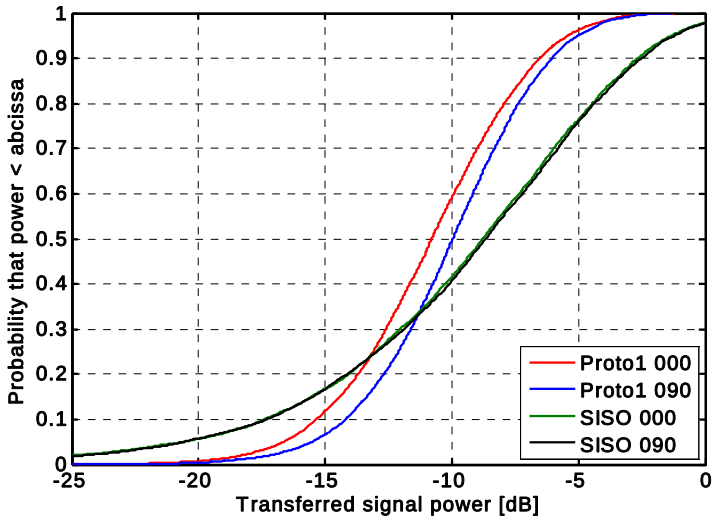

Figure 7.12: *Transferred signal power with the dual-polarized Tx antenna.*

7.4.2 TWO ϕ - POLARIZED TRANSMITTING ANTENNAS WITH DISTANCE OF 0.7 WAVELENGHTS

In these simulations two ϕ-polarized elements of the linear array antenna were used as Tx antennas and the distance between the elements was 0.7 λ. For the single-element reference antenna only one of the elements was used and that is why the results are equal to the SISO results in the previous section. The mutual information results are presented in Figure 7.13. The dual-element prototype has higher mutual information values at all the probability levels than the single-element reference antenna. It can be seen from the result that now the horizontal orientation is better for the dual-element prototype. As discussed above, the radiation pattern is almost horizontally polarized when the antenna is in the horizontal orientation. Now both of the Tx elements are ϕ-polarized and the horizontally oriented antenna receives more signal power than the vertically oriented. At the 10 % outage probability level the maximum mutual information (horizontal orientation) is 320 % higher when using the dual-element prototype compared to single-element reference antenna. At the 50 % outage probability level the difference is 65 %. If the mutual information values with different Tx antennas are compared from Figures 7.10 and 7.13 it can be seen that higher mutual information is obtained when two ϕ-polarized Tx antennas are used. The absolute values of the mutual information results at the 10 % and 50 % outage probability levels are presented in Table 7.1. are presented in Table 7.2.

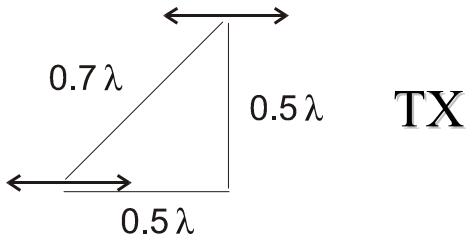

(a)

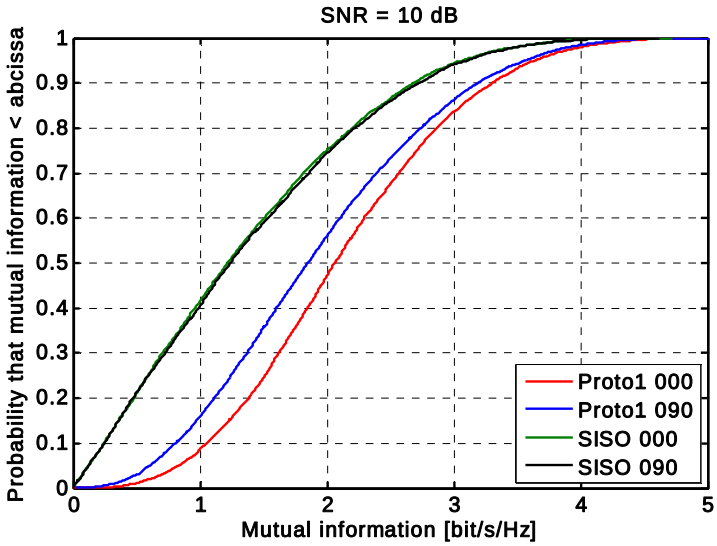

(b)

Figure 7.13: *(a) The configuration of the Tx antennas and (b) mutual information with SNR = 10 dB.*

Table 7.2: *Mutual information with two ϕ-polarized Tx antennas.*

Outage probability level	Mutual information [bit/s/Hz]		
	SISO	Proto1 000	Proto1 090
10 %	0.25	1.05	0.81
50 %	1.25	2.06	1.86

The spatial multiplexing efficiency is presented in Figure 7.14. It can be seen that the spatial multiplexing efficiency is higher when the horizontal orientation is used. When comparing Figures 7.11 and 7.14 the spatial separation of the Tx element does not increase the spatial multiplexing efficiency as much as when using two Tx polarizations.

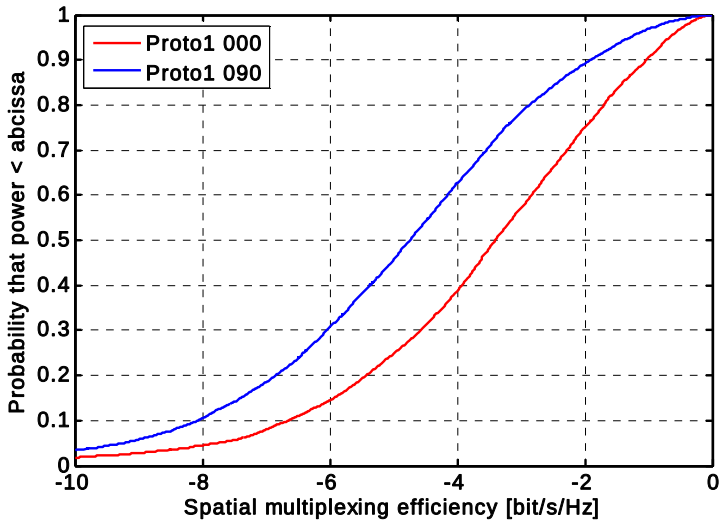

Figure 7.14: *Spatial multiplexing efficiency with two ϕ-polarized Tx antennas.*

In Figure 7.15 the transferred signal power is presented. Higher signal power is achieved with the horizontal orientation of the dual-element prototype. When comparing Figures 7.12 and 7.15 it can be seen that the transferred signal power is about the same in the vertical orientation in both figures. The transferred signal power is a few dB higher in the horizontal orientation when the two ϕ-polarized Tx antennas are used. This is due to the horizontal polarization of the dual-element prototype when the antenna is in the horizontal orientation.

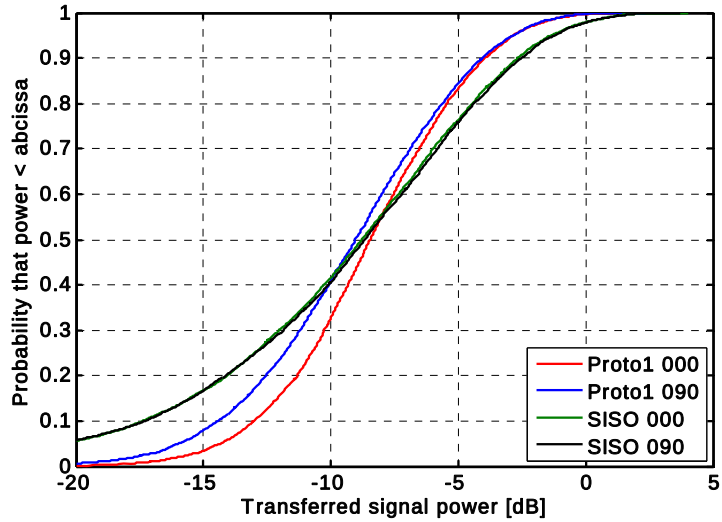

Figure 7.15: *Transferred signal power with two ϕ-polarized Tx antennas.*

7.5 Comments and discussion of the MEBAT results

The MEBAT simulations indicate that higher mutual information can be achieved with dual-element prototype than with the single-element reference antenna. The difference is larger at high reliability levels and if two ϕ-polarized Tx elements are used instead of a dual polarized Tx antenna. If a dual-polarized Tx antenna is used higher mutual information is achieved when the dual-element antenna is in vertical orientation and for two ϕ-polarized Tx elements horizontal orientation is better. Vertical rotation has no effect on the mutual information achieved with single-element antenna.

Although, these results seem promising there are a few things that would require further research. One important thing is the frequency of the channel data that was used in the MEBAT simulations. The frequency was 2 GHz and it is not totally clear that it can be utilized to model the signal environment also at DVB-H frequencies. This could be investigated by doing direct measurements with the dual-element prototype and the single-element reference antenna at 700 MHz and comparing the measurement results with the MEBAT simulation results. The Tx antenna could be e.g. a dual-polarized half-wave dipole or two ϕ-polarized half-wave dipoles. Another aspect is that the matching of the reference antenna is not optimal dual-resonant matching and that is why the results can give too poor impression about the operation of the reference antenna. If the matching would be optimal the realized gain could be about 1 dB higher at 700 MHz and this would increase the mutual information achieved with single-element reference antenna.

8 CONCLUSIONS

The goal of this thesis was to gain knowledge on feasibility of multi-element antennas at DVB-H frequency band. During the thesis, a small planar dual-element antenna structure for handheld DVB-H terminal was designed and a prototype antenna was built. The size of the ground plane is 50 mm x 110 mm (width x length) and the total volume of the antenna is 2 x 1.03 cm^3. The structure of the antenna is based on non-resonant coupling elements which are tuned to the operation frequency range with matching circuits. Three different matching circuits were designed for the prototype. The first single-resonant matching circuit was designed to test the MIMO performance of the antenna with direct measurements at a narrow frequency band in a real signal environment. Two dual-resonant matching circuits were designed to test how the antenna fulfils the DVB-H specification. The first dual-resonant matching circuit was implemented with ideal reactive components and the second with real lumped matching components. Because the antenna is electrically so small a broad bandwidth is difficult to achieve even with a dual-resonant matching circuit. That is why the DVB-H frequency band was divided into two parts and separate matching circuits were designed for both sub-bands. In the final dual-element antenna the desired matching circuit would be chosen with RF switches which were not included in this work.

The most common figure of merit for DVB-H antennas is realized gain. According to simulations with IE3D and measurements the two element prototype antenna fulfils the realized gain specification with a 2.5 dB margin. Losses of the RF switches that would be included to the final antenna were not taken into account in these results. The realized gain was measured at four different frequencies (500, 550, 600 and 670 MHz) and the results agreed well with the simulation results.

Multi-element antennas are often evaluated with envelope correlation coefficient calculated from the 3-D radiation patterns of the antenna elements. Low correlation is desired and it is achieved when the radiation patterns of the antenna elements differ from each other. The radiation pattern of the dual-element prototype is tilted about 40° when the feed is switched from port 1 to port 2. The envelope correlation coefficient of the prototype is under 0.6 at the whole DVB-H band. Usually 0.7 is considered as an upper boundary of the correlation to provide a sufficient diversity performance.

The MIMO performance of the antenna was evaluated with the antenna evaluation tool MEBAT using the 3-D radiation pattern of the dual-element prototype. With MEBAT it was possible to evaluate the antenna in a realistic propagation environment. In the MEBAT simulation 2 GHz channel data was used because propagation data below that frequency was not available. In this work indoor picocell, outdoor microcell and small outdoor macrocell environments were used. A single-element antenna having the same total volume than the dual-element antenna was used as a reference antenna. Simulation results reveal that using a dual-element antenna instead of a single-element antenna can increase mutual information at all outage probability levels. The greatest advantage is gained at high reliability levels where the mutual information of a 2 x 2 MIMO system can be two to four times higher than with a SISO system. Also the effect of the different Tx antennas was examined with MEBAT. It seems that using two ϕ-polarized Tx elements increase mutual information compared to a situation where a dual-polarized Tx antenna is used. These results do not depend much on the used signal environment.

In this thesis it has been shown that sufficiently uncorrelated radiation patterns can be realized with a handheld DVB-H terminal by using coupling element antennas. The advantage of the multi-element antennas can be exploited with MIMO and SIMO systems that can increase link reliability or transmitted data rate.

REFERENCES

[1] H. A. Wheeler, "Small antennas," *IEEE Transactions on Antennas and Propagation*, vol. 23, no. 4, pp. 462-469, July 1975.

[2] H. A. Wheeler, "The radiansphere around a small antenna," *Proceedings of the IRE*, vol. 47, no. 8, pp. 1325-1331, August 1959.

[3] A. Räisänen and A. Lehto, *Radiotekniikan perusteet (Foundations of Radio Engineering, in Finnish)*. Helsinki: Otatieto, 2003, 292 p.

[4] E.Nyfors and P. Vainikainen, *Industrial Microwave Sensors*. Norwood: Artech House, 1989, 351 p.

[5] H.F Pues and A.R. Van De Capelle, "An impedance-matching technique for increasing the bandwidth of microstrip antennas," *IEEE Transactions on Antennas and Propagation*, vol. 37, no. 11, pp. 1345-1354, November 1989.

[6] D.M. Pozar, *Microwave Engineering*. Reading, Massachusetts: Addison Wesley, 1990, 726 p.

[7] J. Ollikainen, *Design and implementation techniques of wideband mobile communications antennas*, doctoral thesis, Helsinki University of Technology, Radio laboratory, 2004.

[8] W. L. Stutzman and G.A. Thiele, *Antenna Theory and Design*. New York: John Wiley & Sons Inc., 1998, 648 p.

[9] H. A. Wheeler, "Fundamental limitations of small antennas," *Proceedings of the IRE*, vol. 35, no. 12, pp. 1479-1484, December 1947.

[10] J. S. McLean, "A Re-examination of the fundamental limits on the radiation Q of electrically small antennas," *IEEE Transactions on Antennas and Propagation*, vol. 44, no. 5, pp. 672-676, May 1996.

[11] A. Lehto and A. Räisänen, *RF- ja Mikroaaltotekniikka (RF and Microwave Engineering, in Finnish)*. Helsinki: Otatieto, 2002, 267 p.

[12] J. Villanen, and P.Vainikainen, "Optimum dual-resonant impedance matching of coupling element based mobile terminal antenna structures," *Microwave and Optical Technology Letters,* vol. 49, no. 10, pp. 2472-2477, October 2007.

[13] IEEE, *IEEE Standard Definitions of Terms for Antennas*, IEEE STD-145, 1993.

[14] J. Villanen, J. Ollikainen, O. Kivekäs, and P. Vainikainen, "Coupling element based mobile terminal antenna stucture," *IEEE Transactions on Antennas and Propagation,* vol. 54, no. 7, pp. 2142-2153, July 2006.

[15] P. Vainikainen, J. Ollikainen, O. Kivekäs, and I. Kelander, "Resonator-based analysis of the combination of mobile handset antenna and chassis," *IEEE Transactions on Antennas and Propagation*, vol. 50, no. 10, pp. 1433-1444, October 2002.

[16] J. Rahola, and J. Ollikainen, "Optimal antenna placement for mobile terminals using characteristic mode analysis," *Proceedings of The European Conference on Antennas and Propagation (EuCAP 2006),* Nice, France, 6-10 November 2006, CDROM., p.146.1

[17] A. J. Paulraj, D. A. Gore, R. U. Nabar, and H. Bölcskei, "An overview of MIMO communications—A key to gigabit wireless," *Proceedings of the IEEE*, vol. 92, no. 2, pp. 198–218, February 2004.

[18] IEEE, "The IEEE standard definitions of terms of antennas," *IEEE Transactions on Antennas and Propagation*, vol. 17, 1969.

[19] Y. S. Yeh, "Antennas and polarization effects," Chapter 3 in *Microwave Mobile Communications*, editor W. C. Jakes, New York: Wiley, pp. 133-158, 1974.

[20] K. Boyle, "Radiation patterns and correlation of closely spaced linear antennas," *IEEE Transactions on Antennas and Propagation,* vol. 50, no. 8, pp. 1162-1165, August 2002.

[21] P. Vainikainen, P. Suvikunnas, and L. Vuokko, "Experimental performance evaluation of MIMO antenna configurations in indoor environments at 5 GHz frequency range," *Proceedings of the European Microwave Association,* vol. 2, no. 3, pp. 218-227, September 2006.

[22] P. Suvikunnas, J. Villanen, K. Sulonen, C. Icheln, J. Ollikainen, and P. Vainikainen, "Evaluation of the performance of multiantenna terminals using a new approach," *IEEE Transactions on Instrumentation and Measurement,* vol. 55, no. 5, pp. 1804-1813, October 2006.

[23] G. J. Foschini, "Layered space-time architecture for wireless communication in a fading environment when using multi-element antennas," *Bell Labs Technical Journal*, pp. 41-59, 1996.

[24] P. Suvikunnas, J. Salo, L. Vuokko, J. Kivinen, K. Sulonen, and P. Vainikainen, "Empirical comparison of MIMO antenna configurations," *Proceedings of the IEEE 61st Semiannual Vehicular Technology Conference*, Stockholm, Sweden, May-June 2005, pp. 53-57.

[25] J. Colburn, Y. Rahmat-Samii, M. Jensen, and G. Pottie, "Evaluation of personal communications dual-antenna handset diversity performance," *IEEE Transactions on Vehicular Technology,* vol. 47, no. 3, August 1998.

[26] J. Villanen, P. Suvikunnas, C. Icheln, J. Ollikainen, and P. Vainikainen, "Performance analysis and design aspects of mobile terminal multi-antenna configurations," *IEEE Transactions on Vehicular Technology,* to be published.

[27] R. Wietfeldt, "Handset system architectures for mobile DTV," *Proceedings of the Tenth International Symposium on Consumer Electronics (ISCE 2006)*, St. Petersburg, Russia, June-July 2006, pp. 1-6.

[28] *DVB Project*, http://www.dvb.org, (cited June 1, 2007).

[29] *Digital Video Broadcasting (DVB); Transmission System for Handheld Terminals (DVB-H)*, ETSI EN 302 304 V1.1.1 (2004-11), European Telecommunications Standards Institute.

[30] P. Talmola, *Handheld Devices and Preferred Spectrum*, http://mmc05.hhi.de/Downloads /3_Technologies_II/Talmola_Hand_Held_Devices_and_Preferred_Spectrum.pdf, (cited September 28, 2007).

[31] *Digital Video Broadcasting (DVB); DVB-H Implementation Guidelines,* ETSI TR 102 377 V1.2.1 (2005-11), European Telecommunications Standards Institute.

[32] J. Holopainen, J. Poutanen, C. Icheln, and P. Vainikainen, "User effect of antennas for handheld DVB terminal," *Proceedings of the ICEAA 2007 International Conference on Electromagnetics in Advanced Applications*, Turin, Italy, 17-21 September 2007, paper number 313.

[33] J. Holopainen, J. Villanen, M. Kyrö, C. Icheln, and P. Vainikainen, "Antenna for handheld DVB terminal," *Proceedings of the IEEE iWAT 2006 Small Antennas and Novel Metamaterials*, New York, USA, 6-8 March 2006, CD-ROM (ISBN 0-7803-9444-5), p. 077.

[34] Pulse Finland Oy, http://www.pulseeng.com/antennas/, (cited June 1, 2007)

[35] J. Holopainen, J. Villanen, C.Icheln, and P.Vainikainen, "Mobile terminal antennas implemented by using direct coupling," *Proceedings of the European Conference on Antennas and Propagation (EuCAP 2006),* Nice, France, 6-10 November 2006, CD-ROM SP-626 (92-9092-937-5), paper: OA17 349858jh.pdf.

[36] P. Vainikainen, J. Ollikainen, O. Kivekäs, and I. Kelander, Pat. FI114260, Radiolaitteen modulaarinen kytkentärakenne ja kannettava radiolaite (Modular coupling structure for a radio device and a portable radio device), Finland, September 15, 2004, 22 p.

[37] J. Holopainen, *Antenna for handheld DVB terminal*, Diploma thesis, Espoo, Helsinki University of Technology, May 2005 , 91 p.

[38] R. Valkonen , *Broadband tuning of small antennas*, Diploma thesis, Espoo, Helsinki University of Technology, March 2007, 85 p.

[39] A. Räisänen and A. Lehto, *Mikroaaltomittaustekniikka (Microwave Measurement Technolgy, in Finnish)*. Helsinki: Otatieto, 2001, 215 p.

[40] K. Sulonen, P. Suvikunnas, L. Vuokko, J. Kivinen, and P. Vainikainen, "Comparison of MIMO antenna configurations in picocell and microcell environments," *IEEE Journal on Selected Areas in Communications*, vol. 21, no. 5, pp. 1-10, June 2003.

[41] K. Kalliola, H. Laitinen, L. Vaskelainen, and P. Vainikainen, "Real-time 3-D spatial-temporal dual-polarized measurement of wideband radio channel at mobile station," *IEEE Transactions on Instrumentation and Measurement*, vol. 49, no. 2, pp. 439-448, April 2000.

[42] P. Suvikunnas, K. Sulonen, J. Kivinen, and P. Vainikainen, "Effect of antenna properties on MIMO-capacity in real propagation channels," *Proceedings of the 2nd COST 273 Workshop on Broadband Wireless Access*, Paris, France, May 21-22, 2003, pp. 1-6.

APPENDIX

INDOOR PICOCELL ENVIRONMENT

DUAL-POLARIZED TX ANTENNA

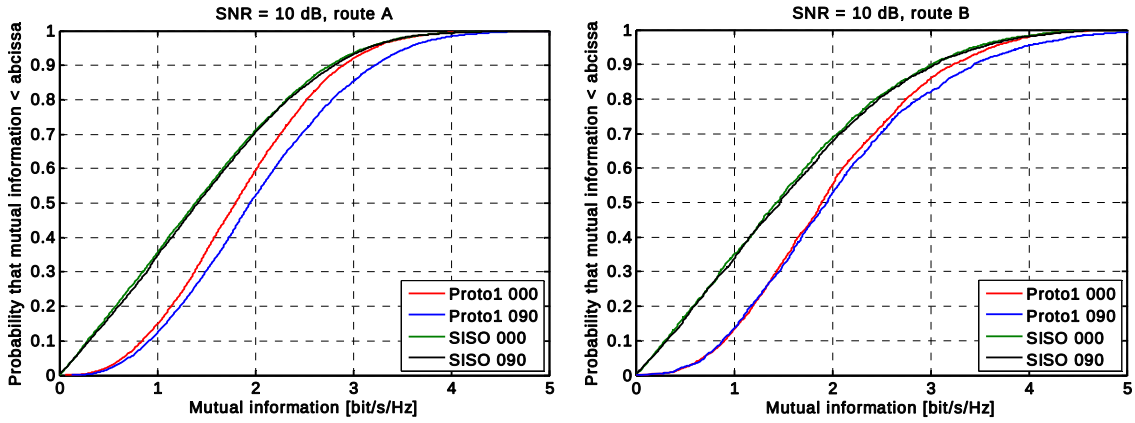

(a) (b)

Figure A.1: *Mutual information for routes (a) A and (b) B with SNR = 10 dB.*

TWO ϕ POLARIZED TX ANTENNAS WITH DISTANCE OF 0.7 λ

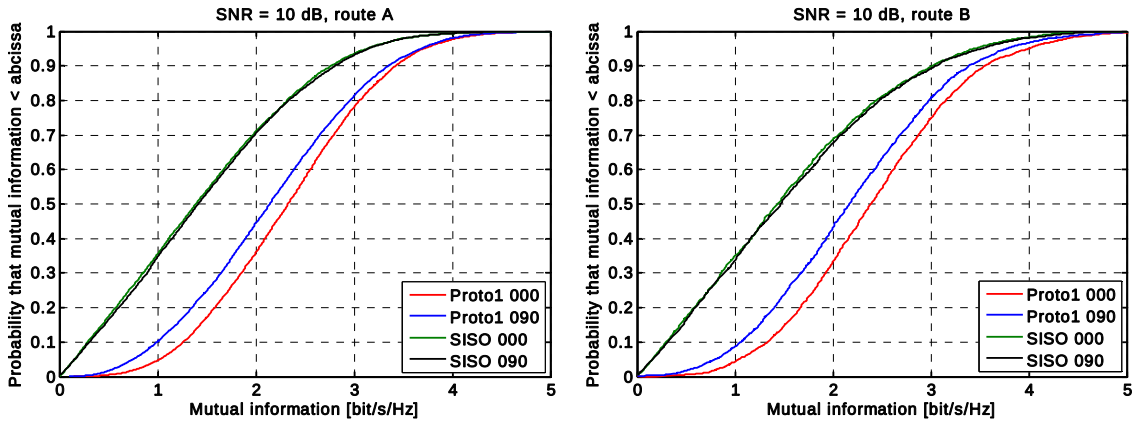

(a) (b)

Figure A.2: *Mutual information for routes (a) A and (b) B with SNR = 10 dB.*

OUTDOOR MICROCELL ENVIRONMENT

DUAL-POLARIZED TX ANTENNA

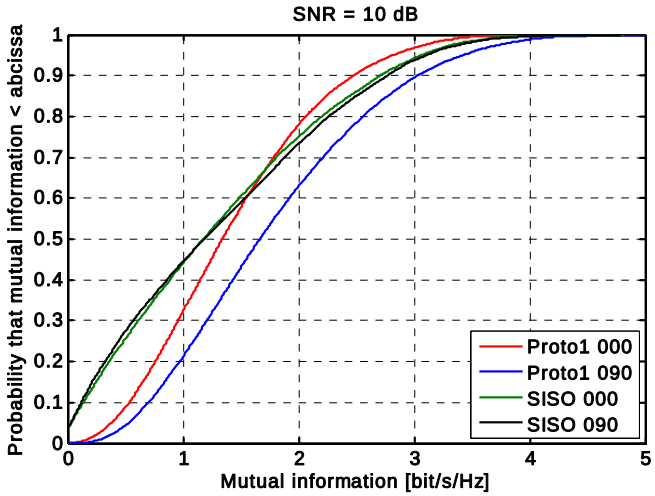

Figure A.3: *Mutual information with SNR = 10 dB.*

TWO ϕ POLARIZED TX ANTENNAS WITH DISTANCE OF 0.7 λ

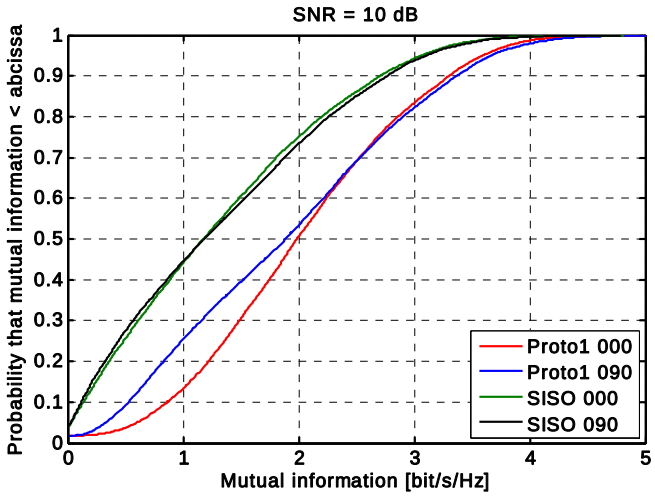

Figure A.4: *Mutual information with SNR = 10 dB.*